Journal of Volcanology and Geothermal Research 444 (2023) 107943

Contents lists available at ScienceDirect

Journal of Volcanology and Geothermal Research

journal homepage: www.journals.elsevier.com/journal-of-volcanology-and-geothermal-research

Origin of the compositionally zoned Paso Puyehue Tephra, Antillanca Volcanic Complex, Chile

Cameron M. DeSilva [a], Brad S. Singer [a,*], Brent V. Alloway [b], Pablo Moreno-Yaeger [a]

[a] Department of Geoscience, University of Wisconsin-Madison, Madison, WI 53706, United States of America
[b] Instituto de Geografía, Pontificia Universidad Católica de Chile, Santiago, Chile

ARTICLE INFO

Keywords:
Bimodal
Tephra
Composition
Holocene
Andes
Antillanca

ABSTRACT

The origin of gaps or zoning in the composition of erupted products is critical to understanding how sub-volcanic reservoirs operate. We characterize the compositionally zoned magma that produced the 2053 ± 50 cal. yr BP Paso Puyehue Tephra from the Antillanca Volcanic Complex in the Andean Southern Volcanic Zone (SVZ). The 3.7 km^3 Paso Puyehue Tephra is zoned from dacite (69 wt% SiO_2) lapilli and ash comprising the lowermost 80% of the deposit that abruptly transitions upward into basaltic andesite scoria (54 wt% SiO_2) making up the remaining ~20%. Variations in whole-rock, matrix glass, and mineral compositions through the deposit allow us to estimate pre-eruptive magma storage conditions and to develop a model of how this magma body was generated.

Our findings suggest that amphibole-bearing basaltic andesitic magma stored at ~8.0 ± 1.3 km depth fractionally crystallized and cooled from 1048 ± 1.1 to 811 ± 28.6 °C under highly oxidizing conditions to produce silicic a melt that upon extraction and rise, pooled at ~6.4 ± 1.2 km depth at temperatures as low as 810 °C before eruption. MELTS models suggest that crystallization of a basaltic andesite parent magma with 4 wt% dissolved H_2O can produce the dacite under conditions predicted by mineral thermobarometers with phase compositions comparable to those measured in minerals. Pervasive normal zoning at the rims of plagioclase crystals—most pronounced at the transition between dacite and basaltic andesite, and compatible vs. incompatible trace element concentrations, suggest that magma mixing was limited and likely occurred at the interface between the dacitic and basaltic andesitic magmas during ascent within the conduit upon eruption. Compositionally bimodal tephras are increasingly recognized throughout the SVZ with several interpreted to reflect basaltic recharge and mixing into extant rhyolitic reservoirs. In further contrast to other SVZ rhyolitic products, e.g., from the nearby Cordón Callue and Mocho Choshuenco volcanoes, the Paso Puyehue magma was highly oxidized. This may reflect enhanced delivery of H_2O from the subducting plate into the mantle wedge, which in turn may facilitate efficient extraction and separation of buoyant, low-viscosity rhyolitic melt from crystal-rich basaltic andesitic parent magmas and the co-eruption of both end members.

1. Introduction

Gaps in the composition of magmas erupted from individual continental arc volcanoes, or within products of singular eruptions that comprise mafic and silicic end members with a paucity of intermediates, have been observed worldwide and puzzled petrologists for decades (e.g., Daly, 1925; Hildreth, 1981, 1983; Bacon and Druitt, 1988; Brophy, 1991; Eichelberger et al., 2000; Hildreth and Fierstein, 2012; Winslow et al., 2022). In continental volcanic arcs, fractional crystallization of basaltic or basaltic andesitic magma is widely recognized as the dominant process that produces strong compositional zoning (e.g., Brophy, 1991; Dufek and Bachmann, 2010; Cooper and Kent, 2014; Wolff et al., 2015; Ganne et al., 2018; Jackson et al., 2018). Physically how, and where, within transcrustal magma plumbing systems this extreme fractional crystallization to produce dacitic to rhyolitic magma occurs remains controversial (Cashman et al., 2017; Winslow et al., 2022). The efficacy of extracting silicic melt from underlying basaltic parent magmas at shallow depths within transcrustal magma plumbing systems has been emphasized at Puyehue-Cordón Caulle in the southern Andes (Seropian et al., 2021; Winslow et al., 2022). Yet, many

* Corresponding author.
E-mail address: bsinger@wisc.edu (B.S. Singer).

https://doi.org/10.1016/j.jvolgeores.2023.107943
Received 25 June 2023; Received in revised form 13 September 2023; Accepted 22 October 2023
Available online 24 October 2023

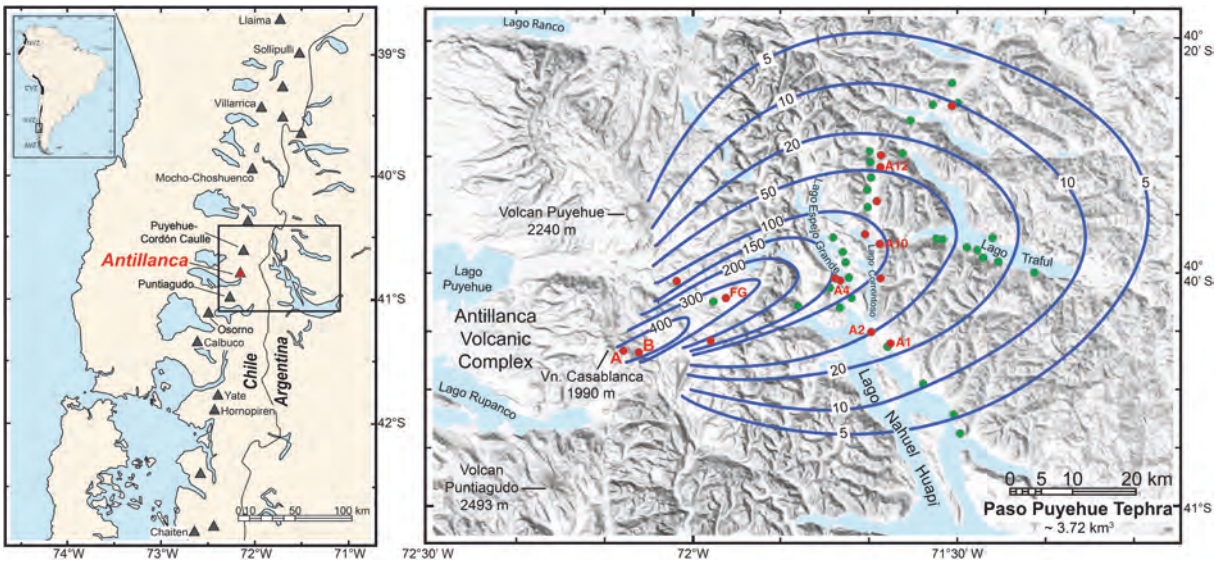

Fig. 1. Regional map of the Southern Andean Volcanic Zone (SVZ) (left) and isopach distribution of the Paso Puyehue Tephra (right; modified from Naranjo et al., 2017). Antillanca Volcanic Complex is located at 41.5°S. Isopach contours in cm. The Frontier gully type section shown in Fig. 2 is denoted FG. Locations of proximal outcrops A and B shown in Fig. 3 are indicated. Tephra sections measured by Alloway et al. (2022) in red dots, sections measured by Naranjo et al. (2017) in green dots, with reference sections A1, A2, A4, A10, and A12 shown in Fig. 4. (For interpretation of the references to colour in this figure legend, the reader is referred to the web version of this article.)

compositionally zoned eruptive products in continental arcs contain evidence that injection of mafic magma and variable degrees of mixing with overlying silicic magma can be important (Bacon and Metz, 1984; Costa and Singer, 2002; Ruprecht et al., 2012; Singer et al., 2016; Alloway et al., 2017; Geoffroy et al., 2018).

The Southern Volcanic Zone (SVZ; Fig. 1) spans 1400 km from 33°S to 46°S and is underlain by crust that thins from 50 km in the north to 35 km south of 37°S (Cembrano and Lara, 2009; Hickey-Vargas et al., 2016; Hildreth and Moorbath, 1988). Within the SVZ, eruptions of compositionally zoned magma are known from Tatara San Pedro volcano (Costa and Singer, 2002), Quizapu volcano (Hildreth and Drake, 1992; Ruprecht et al., 2012), Antillanca volcanic complex (Naranjo et al., 2017; Singer et al., 2008), Michimahuida volcano (Alloway et al., 2017), Melimoyu volcano (Geoffroy et al., 2018) and Puyehue-Cordón Caulle volcano (Winslow et al., 2022).

The aim here is to constrain the pre-eruptive storage conditions and compositional evolution of magma that produced the Paso Puyehue Tephra, deposited by the one of largest late-Holocene eruptions from the Antillanca volcanic complex (AVC). To address this, we determined the composition of (1) whole pumice and scoria samples, (2) matrix glass, and (3) minerals including amphibole, plagioclase, orthopyroxene, clinopyroxene, olivine, and Fe—Ti oxides. In turn, these data are used to constrain the P-T-X-fO_2 conditions of magma storage and crystallization and to ground-truth thermodynamic simulations of magma evolution using the MELTS algorithm.

2. Geologic background

2.1. Antillanca Volcanic Complex (AVC)

The AVC, located 38 km east of the town of Entre Lagos at 40.8°S, is flanked by Lago Puyehue and Lago Rupanco (Fig. 1B) and sits on 35 km thick crust, comprising Oligocene to Pliocene igneous, metamorphic, and sedimentary rocks (Cembrano and Lara, 2009; Hickey-Vargas et al., 2016; Stern, 2004). The AVC differs from nearby arc-front volcanic centers. For example, Puyehue-Cordón Caulle to the north comprises a main composite cone and a rift system and has produced increasingly bimodal eruptions of rhyolite and basaltic andesite during the last 20 ka (Singer et al., 2008; Winslow et al., 2022) and Osorno to the south, which is a large composite cone built mainly of basaltic andesite lavas (Bechon et al., 2022). In contrast, the AVC is a distributed vent complex that has produced several dozen scoria cones and eruptive centers within an area of several hundred km^2 that produced widespread tephra deposits during the Holocene (Singer et al., 2008; Carrasco Lira, 2016; Naranjo et al., 2017; Alloway et al., 2022). The AVC features the late Holocene Casablanca composite volcano, which has a summit vent at 2240 masl and a volume of ~0.7 km^3, >10-fold smaller than other nearby SVZ arc front volcanoes (Mixon et al., 2021). Casablanca and its numerous smaller parasitic cones rest upon deeply eroded stacks of Pleistocene lava and pyroclastic flows that crop out to the southeast and northwest and have erupted mainly basaltic andesite lava flows and scoria during the Holocene (Carrasco Lira, 2016). tephra produced by AVC eruptions are distributed mainly downwind to the east and northeast (Naranjo et al., 2017; Alloway et al., 2022).

The post- Last Glacial Maximum (LGM) tephra deposits in this region of the SVZ are reasonably well-dated and characterized (Alloway et al., 2022). Currently, the interbedded succession of key tephra marker beds is understood to include the: ~11.5 ka Traful Tephra (dacite, ~1.4 km^3), the ~7 ka Espejo Grande dacite Tephra (dacite, ~1.7 km^3), and the ~1.1 ka Mil Hojas rhyodacite Tephra (rhyodacite, ~4.3 km^3)—each sourced from Puyehue-Cordón Caulle—and the compositionally zoned, ~2 ka, Playas Blanca-Negra Tephra (~3.7 km^3), the ~1.9 ka Pampa Frutilla pyroclastic flow, and the subsequent ~7.9 km^3 basaltic andesitic Nahuel Huapi Tephra—each sourced from within the AVC (Alloway et al., 2022; Naranjo et al., 2017).

2.2. The compositionally zoned Paso Puyehue Tephra (PP-T)

Regarding the Playas Blanca-Negra Tephra, Singer et al. (2008) show that the prominent white to black dacitic-basaltic andesitic lapilli and ash fall deposit that Villarosa et al. (2006) named the Nahuel Haupi Tephra, is sourced from the AVC and not from the Puyehue composite volcano whose eastern flanks it drapes (Fig. 1B). The evidence for this conclusion includes $^{87}Sr/^{86}Sr$ ratios that are lower than any determined from Puyehue-Cordon Caulle eruptive products and the presence of amphibole that has not been found in any eruptive product from Puyehue-Cordon Caulle. A ^{14}C date of 2910 ± 150 cal. yr. BP was obtained from soil below this tephra bed by Singer et al. (2008).

Fig. 2. A. Frontier gully type section of the Paso Puyehue Tephra (PP-T) (370 cm thick) located 17.4 km northeast of the proximal outcrops in Fig. 3. B. Base of the PP-T in Frontier gully section located in Fig. 2. C. Transition from dacitic lapilli to basaltic andesite cap. D. PP-T outcrops 600 m southwest of the Frontier gully section from which pumice and scoria lapilli samples PU-04-05 A, B, C, and D (Fig. 4) were collected to determine whole-rock and mineral compositions. Jose Naranjo, Luis Lara, Hugo Moreno, and Brian Jicha for scale.

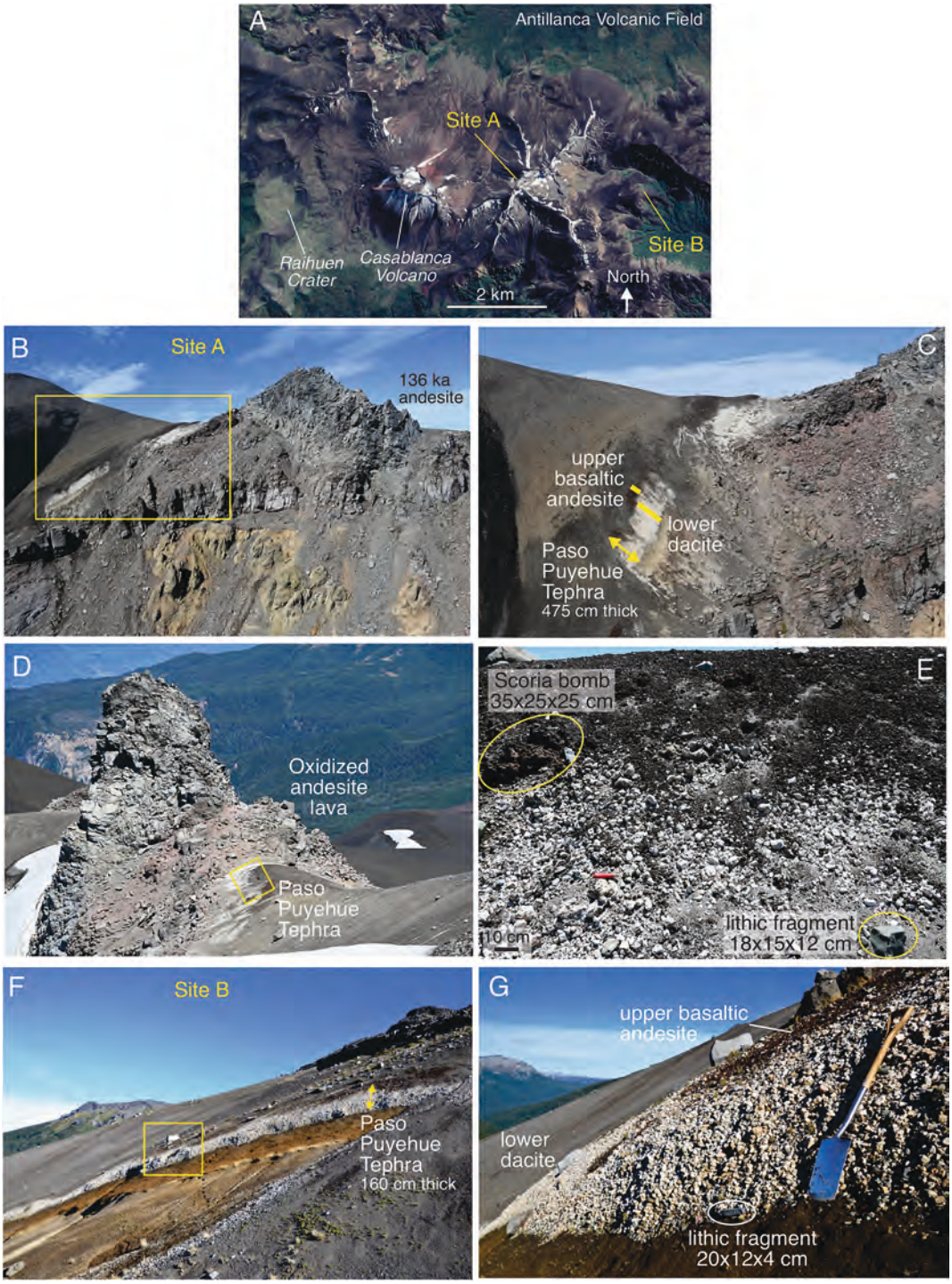

Fig. 3. A. Map (Google Earth) showing the location of two proximal sections of Paso Puyehue Tephra (PP-T) to the east of Casablanca Volcano. B. At site A, PP-T is 475 cm thick and the inset C shows that it rests on pink, oxidized andesite lava $^{40}Ar/^{39}Ar$ dated at 136 ka. E. Close-up of yellow box in panel D showing the coarse size of lithic fragments, dacite pumice clasts, and basaltic andesite scoria bombs. Red knife is 11 cm long. F. Deposit at Site B in panel A, with close-up of the yellow box shown in panel G.

Subsequently, Naranjo et al. (2017) document the areal distribution and volumes of several prominent tephra deposits sourced from Puyehue and the AVC. Naranjo et al. (2017) re-named the distinctive white-to-black zoned tephra marker bed as Playas Blanca-Negra Tephra after its appearance in outcrops. Alloway et al. (2022) noted the cross-border confusion in the regional tephra nomenclature but opted to retain the most recent published name (Playas Blanca-Negra Tephra) for this distinctive compositionally zoned deposit. Alloway et al. (2022) further characterize the composition of glass shards and report an integrated age of 2053 ± 50 cal. yr. BP, based on eighteen ^{14}C dates and highlight its importance as a distinctive regional chronostratigraphic marker.

We here formally designate type and reference sections for the compositionally zoned tephra marker bed and offer a new name, the Paso Puyehue Tephra (PP-T), that satisfies the International Stratigraphic Code which supports the use of unambiguous geographic place names for stratigraphic units (Murphy and Salvador, 1999). The

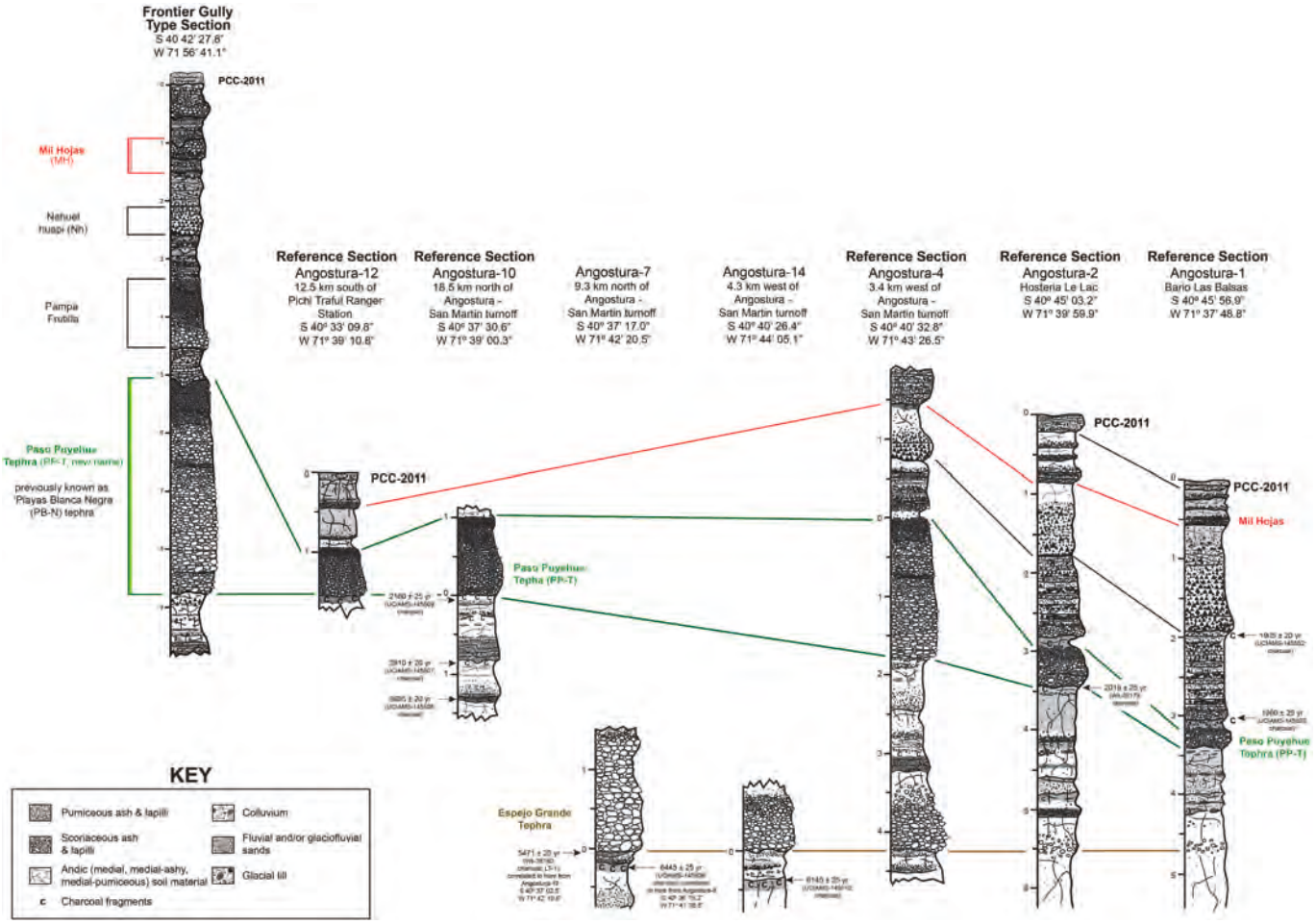

Fig. 4. Frontier Gully type section of Paso Puyehue Tephra showing also reference sections Angostura-1, −2, −4, 10, and − 12 in Argentina located in Fig. 1(sections from Alloway et al., 2022).

proposed type section is just north of the international road over Paso Puyehue (Chile ruta 215), also known as Paso Cardenal Samoré, at the border between Chile and Argentina (Fig. 2A). Since the Paso Puyehue Tephra deposit is laterally continuous with uppermost and lowermost contacts and enveloping stratigraphy intact, we designate the Frontier-1 gully section of Alloway et al. (2022) at 40.707131°S, 71.943890°W, 1337 masl, as its type section (Fig. 1). This section is 17.4 km northeast of the source-proximal section to the east of Casablanca volcano described below and shown in Fig. 3A as site A. At the Frontier gully section (Fig. 2A-C) the Paso Puyehue Tephra is 370 cm thick, with a maximum pumice clast size for the lower dacitic unit of 6.2 × 4.6 cm and for the upper mafic sub-unit, the maximum scoria size is 7.4 × 6.7 cm.

Building on the work of Naranjo et al. (2017) and Alloway et al. (2022), we discovered a source-proximal outcrop of Paso Puyehue Tephra >475 cm thick comprising exceptionally coarse blocks of dacitic pumice up to 30 cm in diameter, overlain by agglutinated scoria bombs of similar dimensions at localities, between 2.5 and 4.0 km east of the Casablanca cone within the AVC (Figs. 1 and 3). At this locality, the 475 cm thick deposit rests on a late Pleistocene andesitic lava flow that has been thermally oxidized to a pink colour, indicating deposition of hot Paso Puyehue Tephra (e.g., Moore et al., 2022; Fig. 3 B-E). In both proximal sections, singular lithic fragments up to 30 cm are common in the basal dacitic portion of the Tephra, as is a lithic-rich dacitic ash bed at the base suggesting a precursory vulcanian-type explosive eruption. Moreover, Paso Puyehue Tephra does not crop out to the west of these two proximal sites. These observations lead us to infer that the vent for the eruption that produced the Paso Puyehue Tephra is between these two sites and has been obscured by erosion and burial under later scoria and ash fall deposits sourced from the Casablanca volcano as well as ubiquitous neoglacial till deposits (Fig. 3A).

In addition to the Frontier gully type section, reference sections that include the Paso Puyehue Tephra in Argentina include the Angostura-1, −2, −4, −10, and − 12 sections of Alloway et al. (2022) located in Fig. 1, and illustrated in Fig. 4.

3. Samples and methods

Four samples of pumice and scoria lapilli that span the vertical extent of the Paso Puyehue Tephra were collected from a site designated PU-04-05 northwest of the Paso Puyehue along Chilean Route 215 at 40.70952°S, 71.94737°W, 1271 masl, that is about 600 m southwest of the Frontier-1 gully section (Fig. 2D). At the proximal sites described above, the Frontier gully section, and the PU-04-05 section, an underlying lithic-rich ash layer is conspicuous (Fig. 2B). Above this ash layer, at the PU-04-05 section, the lowermost 390 cm of the deposit comprises white pumice lapilli overlain by a 10 cm thick layer of mixed or rarely banded tan-gray lapilli, that in turn is overlain by 70 cm of dark scoria lapilli and rare lithic clasts that fines upwards. Sample PU-04-05 A comprises vitric dacitic lapilli from 100 cm above the base of the tephra, PU-04-05 B comprises vitric dacitic lapilli from 350 cm above the base of the deposit, PU-04-05C comprises mingled lapilli from the transitional layer, and PU-04-05 D is from the more crystal-rich dark brown scoria that caps the deposit (Figs. 3D and 5). Vesicles are well-formed and elongated in the white pumice clast, becoming more irregular and less

Fig. 5. Paso Puyehue Tephra pumice and scoria lapilli collected from the section in Fig. 3D from which whole-rock and mineral compositions were determined. PU-04-05 A is lapilli from the lower 270 cm of the Paso Puyehue dacite, PU-04-05 B comprises the top 50 cm of the dacite, PU-04-05C is limited to lapilli from the ~5 cm transition from dacite to basaltic andesite and exhibits rare streaks of light and dark colored glass. PU-04-05 D is from the scoriaceous basaltic andesite that caps the deposit. The yellow scale is in cm and is similar for each panel.

abundant in the scoria. The pumice samples contain fewer than 10 modal percent crystals of amphibole, plagioclase, two pyroxenes, Fe—Ti oxides, and very rare olivine whereas the scoria sample contains the same phases at a much higher ~25% mode (Fig. 6).

Whole-rock major and trace element compositions of the four samples were measured at Hamilton Laboratories by X-Ray fluorescence (XRF), and inductively coupled mass spectrometry (ICP-MS) respectively (Conrey et al., 2023; Mixon et al., 2021). Whole-rock major and trace element compositions are in Table 1; methods and standards are in Supplementary Materials Table S1.

Mineral and glass compositions were measured using a Cameca SX-Five Field Emission Electron Probe Microanalyzer (EPMA) at the University of Wisconsin-Madison Department of Geoscience. Polished mounts of amphibole, clinopyroxene, orthopyroxene, magnetite, ilmenite, olivine, and glass were prepared for each sample in Fig. 5. Plagioclase was measured in situ in polished thin sections. EPMA analyses were performed at 15 keV with a 10 μm diameter beam. Glass shards were measured at 15 keV with a 6 μm diameter beam to minimize damage and avoid microlites. X-ray data were acquired and processed using Probe for EPMA software and calibrated using natural and synthetic standards (Supplementary Materials Table S2).

4. Results

4.1. Mineralogy, petrography, and geochemistry

Mineral phases range from microlites (<10 μm) within the interstitial glass to crystals up to 3 mm in length including plagioclase, euhedral amphibole, clinopyroxene (cpx), orthopyroxene, titanomagnetite, ilmenite and trace amounts of olivine in the dacitic and andesitic portions of Paso Puyehue Tephra. Orthopyroxene is absent in the basaltic andesite portion of the deposit that contains instead olivine. The relative abundances of phases change through the transition from dacite to basaltic andesite units: plagioclase, cpx, opx, oxides, and olivine are more abundant, and amphibole is less abundant and has reaction rims in the basaltic andesite (Fig. 6). The basaltic andesite portion of the Paso Puyehue Tephra contains about 5 vol% lithic fragments, whereas they are less abundant (2–3 vol%) in the dacite, except as noted at the base of the deposit in proximal locations. Euhedral amphibole crystals up to 2 mm long comprise ~1% of the dacite pumice and are present in trace amounts in the basaltic andesite scoria.

Polished thin sections of each sample of Paso Puyehue Tephra (Fig. 5) reveal that the pumice and scoria are highly vesiculated, with elongated tubular vesicles characteristic of the dacite. Plagioclase, titanomagnetite, amphibole, and apatite inclusions are ubiquitous with olivine, cpx, and opx increasing in abundance stratigraphically up section. The Paso Puyehue dacite is crystal-poor but the glass contains abundant microlites (Alloway et al., 2022). The dacite contains amphibole that is rarely zoned and normally zoned plagioclase often as large euhedral crystals (Fig. 6F). Plagioclase with diffuse oscillatory zoning (Fig. 6H) or sieve textures are rare in the dacite. Plagioclase with dominantly normal zoning, rare diffuse oscillatory zoning, and largely unzoned amphibole crystals likely reflect the monotonic cooling of magma (Humphreys et al., 2006). The Paso Puyehue basaltic andesite is less vesicular and relatively more crystal-rich than the dacite. In the basaltic andesite, normal zoning (Fig. 6B), and sieve textures (Fig. 6D) are common in plagioclase, as is sector zonation in pyroxenes. Rare multi-phase glomerocrysts (Fig. 6C), most commonly plagioclase with cpx or opx, up to 1 mm in diameter occur in the andesite and basaltic andesite and may be remnants of crystal mush from the floor or walls of the magma reservoir (e.g., Winslow et al., 2022). Amphiboles lack reaction rims in the dacite through transitional samples (Fig. 6E, G), however many in the basaltic andesite scoria have ~10–15 μm thick reaction rims of pyroxene and oxides (Fig. 6A).

Whole-rock (Table 1) and glass compositions indicate that the basal pumice is dacite (67–69 wt% SiO_2), the capping scoria is basaltic

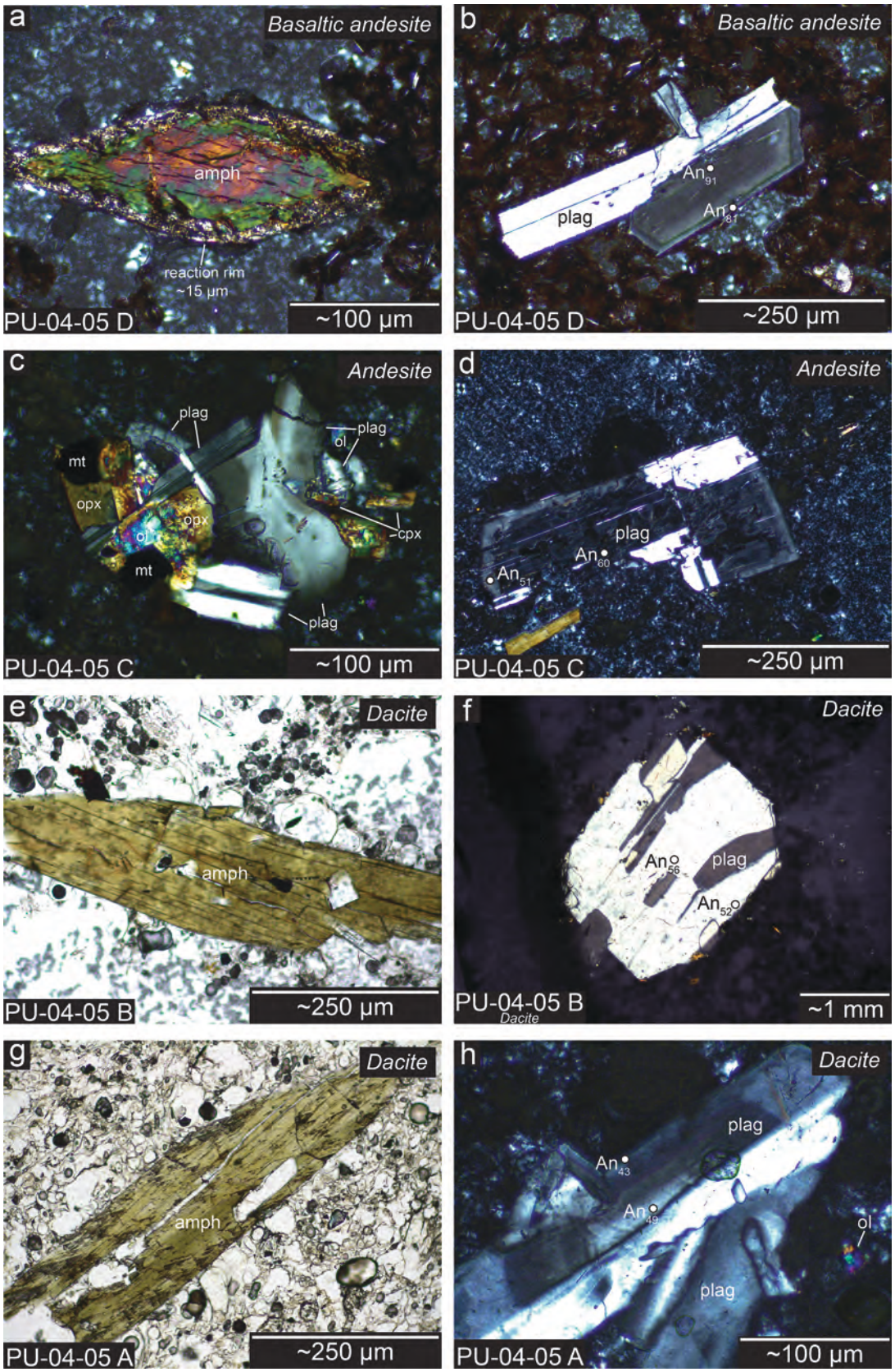

Fig. 6. Representative thin section photomicrographs for each Paso Puyehue Tephra sample in stratigraphic order (Fig. 4). A. Amphibole with a ~ 15 µm reaction rim. B. Normally zoned plagioclase. C. Glomerocryst of plagioclase, cpx, opx and olivine. D. Plagioclase displaying sieve texture and normal zoning. E. Euhedral amphibole. F. Large, euhedral, normally zoned plagioclase. G. Euhedral amphibole without reaction rim. H. Normally zoned plagioclase.

Table 1
Whole-rock major and trace element composition of Paso Puyehue Tephra samples (Figs. 2D and 4). Uncertainties of oxide and trace element concentrations are < ± 0.2% (1σ).

Sample:	PU-04-05 A	PU-04-05B	PU-04-05C	PU-04-05D
cm above base	100	350	375	400
(wt%)				
SiO_2	68.45	66.72	61.11	53.73
TiO_2	0.41	0.47	0.74	1.06
$Al2O_3$	15.11	15.58	16.91	18.16
FeO*	2.51	3.16	5.27	8.42
MnO	0.09	0.10	0.13	0.16
MgO	0.70	1.04	2.16	4.15
CaO	2.54	3.16	5.13	8.31
Na_2O	4.67	4.61	4.45	3.76
K_2O	2.57	2.37	1.75	0.89
P_2O_5	0.12	0.17	0.28	0.24
LOI (%)	1.97	2.05	1.29	0.43
sum	99.41	99.74	99.51	99.53
volatiles (wt%)				
F	0.02	0.03	0.00	0.00
Cl	0.11	0.12	0.11	0.04
SO_3	0.00	0.03	0.04	0.03
(ppm)				
Br	3.47	3.57	3.16	2.26
As	2.55	0.00	5.92	3.38
Trace elements (ppm)				
Ni	3.2	4.6	8.0	19.0
Cr	1.7	2.0	9.3	30.5
V	28.1	45.3	112.9	238.0
Sc	4.9	6.0	14.0	28.5
Cu	10.0	12.3	26.5	89.7
Zn	50.9	56.9	73.9	84.0
Ga	14.4	15.8	18.4	17.4
Ba	628.8	598.5	465.4	265.3
Rb	72.6	66.0	42.8	16.7
Cs	3.8	2.7	2.0	0.3
Sr	316.9	373.3	499.3	541.0
Y	17.2	17.0	21.5	21.1
Zr	163.0	155.6	135.5	99.8
Hf	4.1	3.3	3.4	2.5
Nb	4.8	2.4	3.4	3.2
Ta	0.8	0.8	0.8	0.9
Mo	3.7	2.9	1.6	2.0
La	15.9	19.6	14.9	10.6
Ce	40.0	36.3	32.5	34.5
Nd	16.1	15.9	19.2	15.0
Sm	2.9	2.8	4.0	3.3
Dy	3.2	3.4	4.1	3.7
Yb	2.0	1.9	2.1	2.2
Th	11.4	8.7	8.4	3.8
U	0.8	1.9	0.5	0.8
Tl	0.6	0.0	0.0	0.0
Pb	17.3	15.0	13.2	6.8
Sn	0.0	3.4	0.5	3.8
Bi	0.0	0.0	0.0	0.0
Sb	1.5	1.7	1.8	1.1

andesite (54 wt% SiO_2) and the transitional pumice is andesite (61 wt% SiO_2; Fig. 7). Matrix glass compositions from the four samples in Fig. 5 are richer in SiO_2 and total alkalis and poorer in MgO than the whole-rock compositions. This reflects the abundance of mineral phases present within evolved glasses that represent residual melt compositions in the magma reservoir quenched upon eruption (Fig. 7).

The variation of select trace element (TE) concentrations in whole-rock (squares; Table 1) and glass shards (circles; Alloway et al., 2022) reveal that Hf and Zr monotonically increase together, whereas Cr declines as Zr increases (Fig. 8). Rb concentrations in the whole-rocks and glass shards generally decline as Sr decreases, although glass shard analyses containing more than ~650 ppm Sr may be biased by plagioclase microlites (Alloway et al., 2022; Fig. 8). Dy and Yb concentrations in the four whole-rock samples are similar, yet the glass shards exhibit a negative correlation between Dy/Yb and Yb (Fig. 8).

4.2. Mineral compositions

Plagioclase compositions range from An_{42} to An_{65} in both samples of Paso Puyehue dacite, in contrast to those from the andesitic lapilli that range widely from An_{38} to An_{90} (Fig. 9A and B). Plagioclase in the basaltic andesitic scoria (Fig. 5D) are more calcic and range from An_{65} to An_{91}, although most cores and rims tightly cluster around An_{90} (Fig. 9A and B). Olivine compositions range from Fo_{77} to Fo_{83}, including exceptionally rare crystals in the dacitic lapilli (Fig. 9C). Amphiboles plot as hornblende to tschermakite to pargasite, without significant systematic differences between core and rim compositions (Fig. 9D). Some amphiboles are normally zoned, with higher Al and Mg numbers in cores relative to rims (Supplementary Materials Table S4 - Amphiboles). Pyroxene compositions largely overlap among the four samples. Cpx is largely augite, whereas opx is enstatite (Fig. 9E).

Plagioclase crystals from the two dacitic samples and the andesitic sample are dominantly normally zoned, and few feldspars in the basaltic andesite are normally zoned (Fig. 10). Plagioclase cores in the dacite are most frequently ~An_{55}, whereas rims are ~An_{50}. No significant difference in plagioclase composition is observed between samples of Paso Puyehue dacite. Plagioclase cores and rims in the basaltic andesite are most frequently between An_{88} and An_{92}, with a few overgrown by thin rims of An_{65} to An_{80}. Plagioclase in the andesitic pumice sample posses the largest core-rim compositional shifts with rims of An_{40} to An_{64} mantling cores of An_{46} to An_{66}. Moreover, in this sample, a handful of plagioclase core compositions are $An_{85–90}$, similar to plagioclase from the basaltic andesite, wheras plagioclase rims are comparable to those in the dacite. The middle transect in Fig. 10 shows a plagioclase with an An_{90} core overgrown by a ~ 15 μm thick An_{65} rim. This crystal likely nucleated in basaltic andesitic melt and was entrained immediately prior to eruption into the dacite and thus records generation of hybrid andesitic magma. In the dacite samples, plagioclase cores are consistently higher in anorthite than the rims, consistent with a simple cooling history from high to low temperature. Similarly, we infer that the rare olivine crystals found in the andesite and dacite pumice likely grew in the basaltic andesitic magma represented by sample PU-05-04D and were incorporated into the dacite during eruption.

4.3. Thermobarometry

Temperature, pressure, oxygen fugacity, and water content associated with crystallization are estimated from the composition of i) euhedral crystal rims, ii) minerals that show no resorption or disequilibrium textures, and iii) minerals that meet the criteria for chemical equilibrium based on measured partition coefficients (K_D) for the elements of interest (Putirka, 2008). Thermobarometry requiring a liquid composition is performed with bulk-rock for liquid composition, whereas that requiring H_2O input used the average weight % H_2O estimated from iterating the plagioclase-liquid hygrometer of Waters and Lange (2015). We report averages of multiple measurements in Fig. 11.

We calculate plagioclase-liquid temperatures and H_2O contents by iterating eq. 23 of Putirka (2008) with the hygrometer of Waters and Lange (2015) using the Python3 tool Thermobar (v1.0.9; Wieser et al., 2022). We use only rim compositions of euhedral plagioclase in calculating H_2O content and temperatures. The temperature and pressure at which amphibole crystallizes are estimated using Ridolfi (2021) and are compared to those estimated using Putirka (2016). Clinopyroxene-liquid, orthopyroxene-liquid, and two pyroxene temperatures and pressures are calculated using Putirka (2008) and we use the two-pyroxene matching algorithm and iterative algorithms for cpx-liquid and opx-liquid of Wieser et al. (2022) for pairs that satisfy high-T and low-T K_D, as suggested by Putirka (2008). The temperature of the

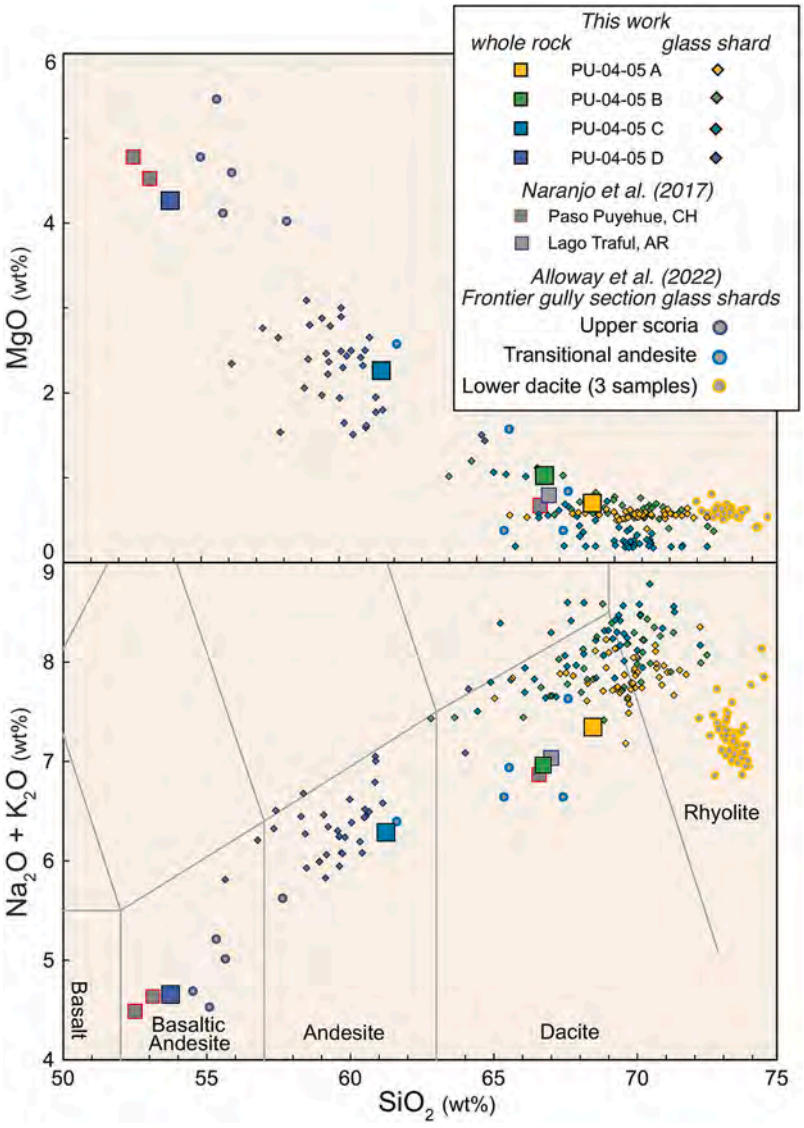

Fig. 7. Major element variation diagrams of bulk-rock (squares) and glass compositions (colored diamonds) from the four samples in Fig. 5. Whole-rock compositions from Naranjo et al. (2017; dark gray squares) and glass shard compositions from Alloway et al. (2022) (light gray circles with colored borders) are also plotted.

basaltic andesite (Sample PU-05-04D) is calculated using the olivine-liquid thermometer of Putirka (2008) with pressure input from Ridolfi (2021). We estimate Fe—Ti oxide temperatures and oxygen fugacity using Ghiorso and Evans (2008). Most estimates are based on touching oxide pairs, but we also use some non-touching pairs such that the Bacon and Hirschmann (1988) test is met (Supplementary Materials Table S8). The Fe^{2+}/Fe^{3+} distribution is estimated using Droop (1987).

To estimate the temperature and depth at which sub-volcanic magma bodies are stored and crystallized using mineral-melt equilibria it is important to recognize that pressure estimates are co-dependent on temperature and H_2O contents and vice-versa. Accordingly, pressure-temperature estimates were refined by iterations of individual geo-barometers, geothermometers, and hygrometers. We use the iterating algorithms of Wieser et al. (2022) in pyroxene and plagioclase thermobarometry to reduce the dependence on other thermobarometer results for inputs (Supplementary materials, Tables S3 to S8).

Fig. 11 summarizes estimates of pre-eruptive pressure and temperature obtained from minerals in the four samples. Depth was calculated from pressure by assuming a constant 2.7 g/cm^3 crustal density. These estimates suggest that the dacitic magma crystallized at lower temperatures and pressure than the basaltic andesite.

The 800–850 °C temperatures from Fe—Ti oxides (Ghiorso and Evans, 2008) are lower than other thermometers and are consistent with ilmenite crystallizing later during cooling than the other phases. Plagioclase-liquid hygrometry suggests a dissolved melt H_2O content of 3.5–4.0 wt%, consistent with MELTS numerical models presented below.

Because it is a recent calibration applicable to calc-alkaline systems, and is a single-phase, temperature-independent barometer, we favor pressure estimates from the Ridolfi (2021) amphibole barometer. The latter gives pressure estimates that are similar to, or only slightly higher than the Putirka (2008) two-pyroxene barometer (Fig. 11). In contrast, the Putirka (2016) amphibole+liquid barometer yields an unrealistic range of pressures corresponding to a magma body >5 km thick (Fig. 11). Pressure estimates from amphibole (Ridolfi, 2021) constrain depth to about 6.5 km in the dacite and 8 km in the basaltic andesite. These depths are consistent with the proposal of Rasmussen et al. (2022) that hydrous arc magmas may exolve and lose H_2O, increase in viscosity, and pond well below depths of neutral buoyancy.

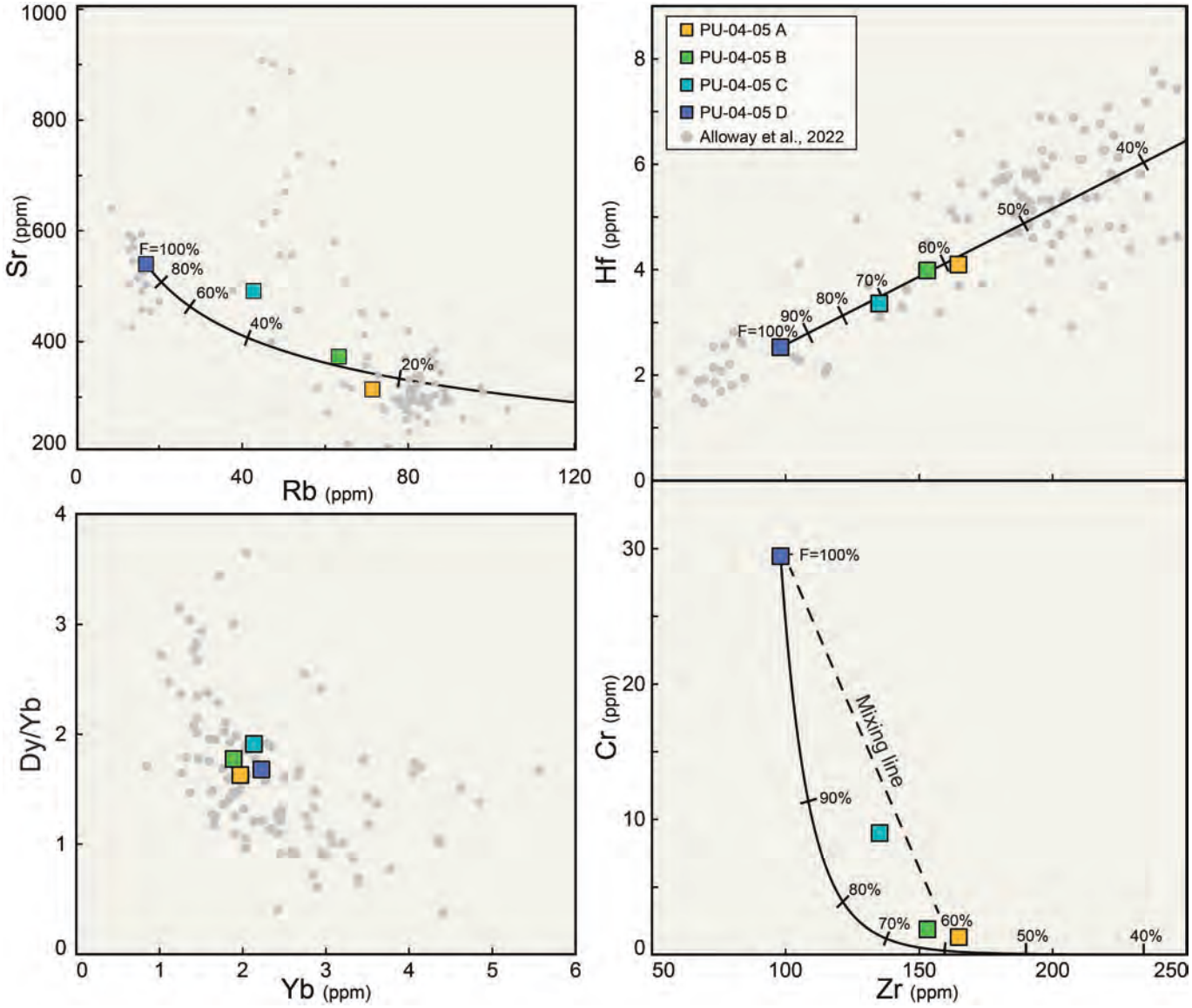

Fig. 8. Trace element variation of Paso Puyehue Tephra samples shown in Figs. 3D and 4. Glass shard data obtained using laser ablation ICP-MS (Alloway et al., 2022) are plotted where possible (gray circles). Taking the composition of sample PU-04-05 D as a parent magma, Rayleigh fractional crystallization models produce the observed dacite composition via ~40 wt% fractionation of olivine, plagioclase, two pyroxenes, oxides, and amphibole (F = % melt remaining in the models). Additional crystallization may explain the Zr-rich interstitial glass compositions. The intermediate composition pumice (sample PU-04-05C) may be better explained by *syn*-eruptive mixing of basaltic andesite and dacite. Glass analyses >650 ppm Sr are likely due to the incorporation of microlitic plagioclase in ICP-MS analyses.

5. Discussion

5.1. Models of magma reservoir evolution

Simple Rayleigh fractional crystallization models of trace element evolution are compared to observed concentrations in whole-rocks and matrix glasses in Fig. 8. From the mineral assemblage in the basaltic andesite scoria, whose whole-rock composition is assumed to be a parent magma, bulk distribution (D) values of 0.05 are used for incompatible elements Hf, Zr, and Rb, a value of 1.3 for Sr, which is strongly compatible in plagioclase, and a value of 10 for Cr which is compatible in olivine. The models including Hf, Zr, and Cr indicate that the dacite bulk composition can be generated via 40 wt% fractionation of a cumulate mineral assemblage including plagioclase, olivine, opx, cpx, Fe—Ti oxides, and amphibole. Moreover, crystallization of an additional 20 wt% cumulate can generate the Hf and Zr-rich rhyolitic melts that comprise the residual glass in the dacite pumice (Figs. 7 and 8). The decline in Dy/Yb with increasing Yb in the spectrum of glass shard compositions, coupled with the decline in Sr with increasing Rb observed in the whole-rock and glass compositions of the basaltic andesite to the dacite components reflects crystallization of amphibole and plagioclase (e.g., Davidson et al., 2007; Fig. 8). The Rayleigh model for Rb and Sr requires more extreme crystallization of the basaltic andesite parent magma than the other models in Fig. 7 and this may reflect the accumulation of plagioclase in the basaltic andesite that would lower its Rb and raise its Sr concentrations. The andesitic sample does not follow the Rayleigh fractionation model trends in the Cr vs. Zr and Sr vs. Rb diagrams, hinting that this small portion of the Paso Puyehue Tephra reflects mixing between the dacitic and basaltic andesitic end member compositions (Fig. 7). Plagioclase with An_{90} cores overgrown with thin An_{64} rims found in the andesitic pumice (Fig. 10) is consistent with *syn*-eruptive mixing of the dacitic and basaltic andesitic magma.

Numerical phase equilibrium experiments are executed using MELTS software (v.1.2.0; Ghiorso and Sack, 1995; Asimow and Ghiorso, 1998) to explore possible pre-eruptive magma storage conditions and

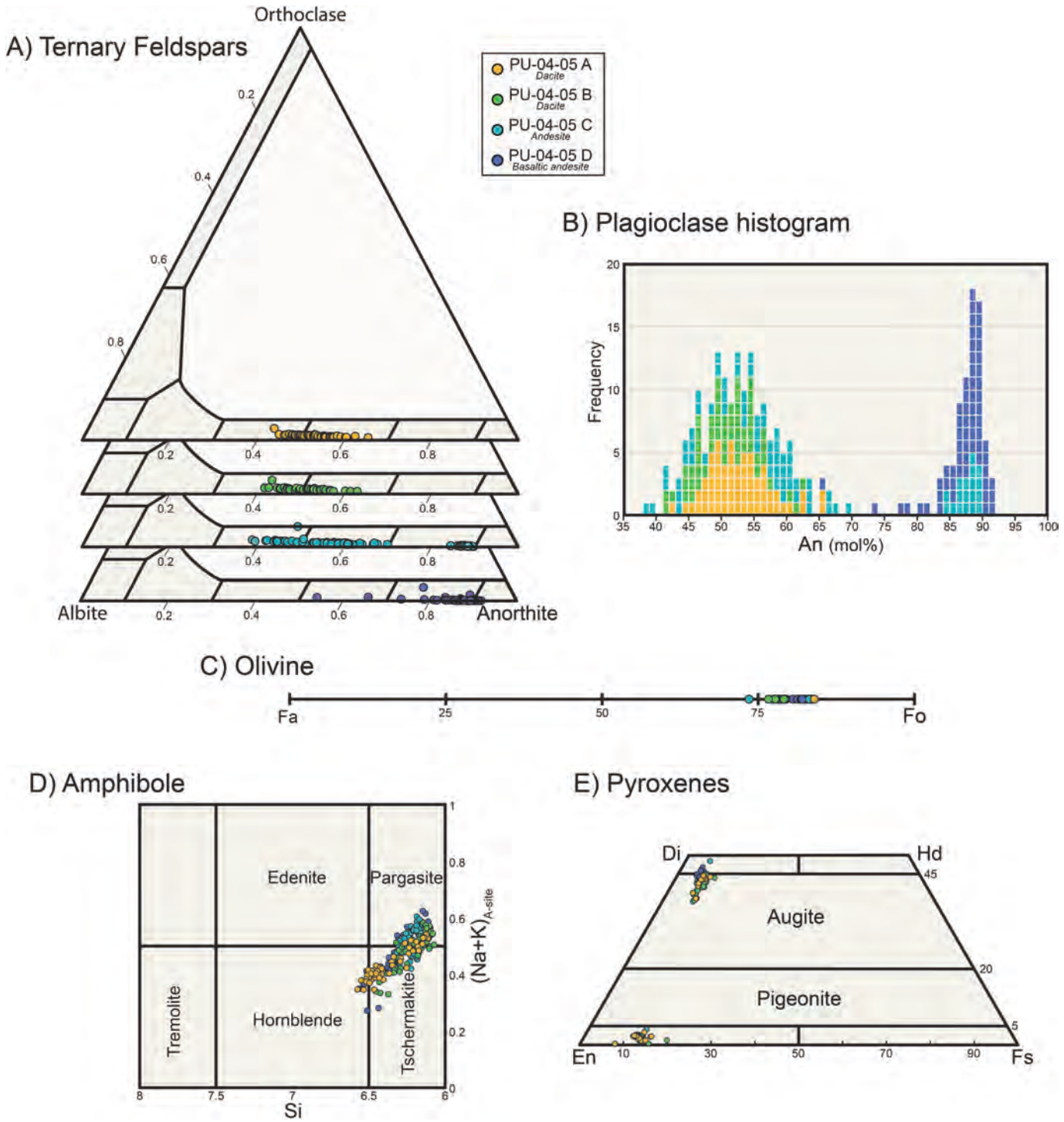

Fig. 9. Mineral compositions from four Paso Puyehue Tephra samples in Fig. 5. (A) feldspar ternary diagram, (B) feldspar anorthite content distribution in histogram, (C) olivine, (D) amphibole compositions, (E) pyroxene quadrilateral.

compositional evolution. We simulated a range of scenarios to determine whether the dacitic and rhyolitic melts (Figs. 7 and 8) may derive from the crystallization of a basaltic andesite parent magma with a composition similar to sample PU-04-05 D (Table 1), and if so, what mineral and melt phases are involved and under what conditions might this occur. Isobaric fractional crystallization experiments, cooling from 1200° to 750 °C were executed at the QFM + 2 oxygen buffer and 2.5 kbar pressure, consistent with thermobarometer estimates of oxygen fugacity and pressure (Figs. 11 and 12; Table 2). Eight models have been generated assuming a range of H_2O content in the starting melt from 0 to 5 wt%.

The MELTS model of isobaric fractional crystallization with a liquid line of descent that best matches observed bulk compositions at 2.5 kbar pressure contains 4% H_2O in starting melt, corresponds to 500 °C of temperature drop, and records ~60 wt% crystallization of the parent magma (Fig. 13). Rayleigh models require only ~40 wt% crystallization to evolve the trace element composition of the basaltic andesite to that similar to the dacite, while another 20 wt% crystallization reaches the trace element composition of glasses (Fig. 8). This additional 20 wt% crystallization required to reproduce the liquid trace element

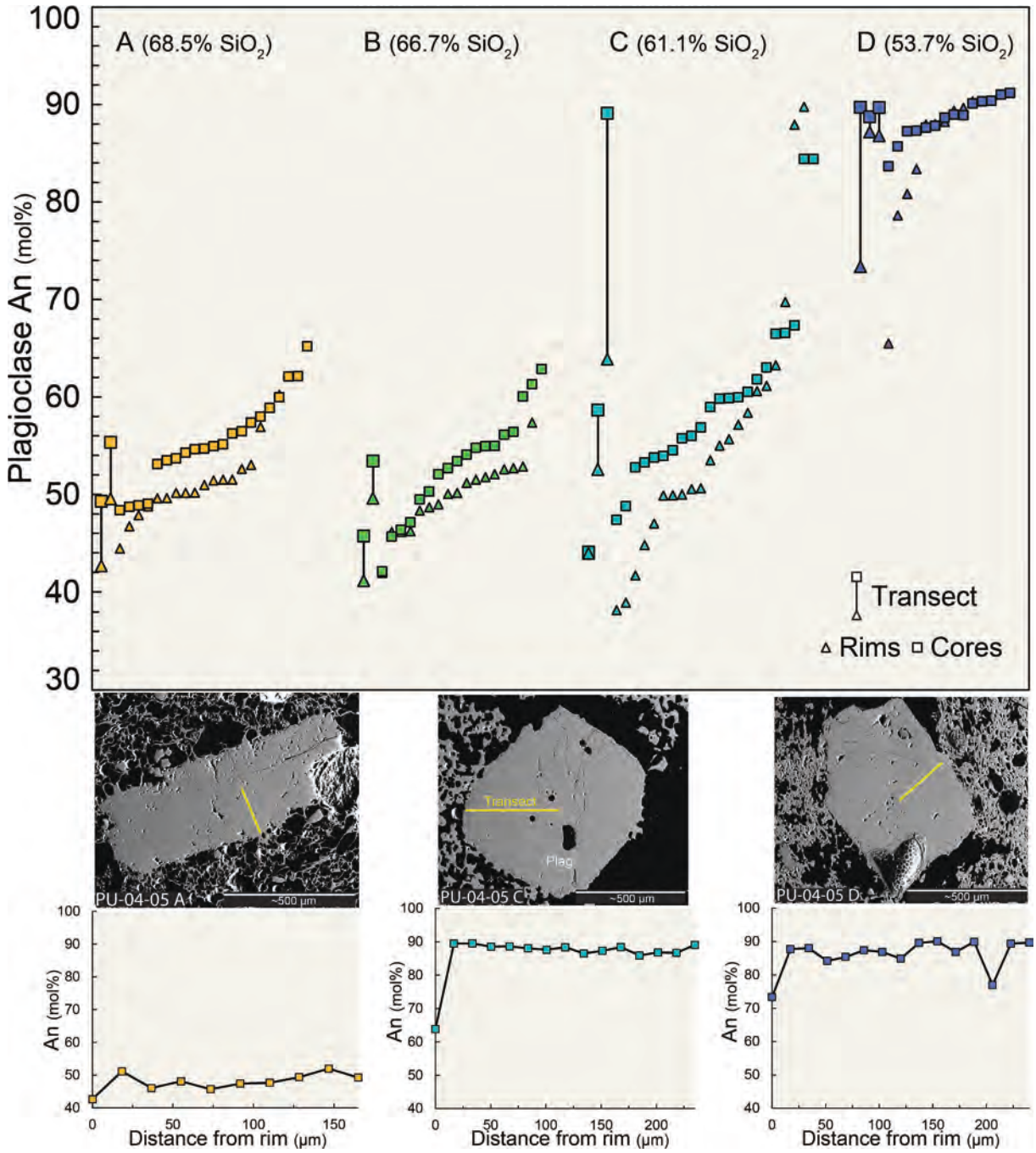

Fig. 10. Anorthite content of plagioclase from each sample of Paso Puyehue Tephra in rank-order plot. Three typical feldspar transects from base, transition, and top of the Paso Puyehue Tephra are shown. Individual analyses are displayed as spots (rims = triangles, cores = squares), and core-to-rim transects are along the yellow lines in the backscattered electron images. Note the absence of reversely zoned plagioclase d the crystal from the intermediate composition sample with a thin rim of An_{64}, mantling a core of An_{90} (middle transect). We interpret the latter crystal as having grown in the basaltic andesite magma prior to transfer into the dacite magma during conduit ascent. (For interpretation of the references to colour in this figure legend, the reader is referred to the web version of this article.)

composition is largely consistent between models and reasonable for a liquid line of descent (Grove and Baker, 1984). Four wt% H_2O is consistent with the highest estimates of dissolved magmatic water from plagioclase-liquid hygrometry (Table 2; Waters and Lange, 2015). The fractionated minerals include magnetite, plagioclase, cpx, opx, amphibole, and ilmenite (Fig. 13). Comparable MELTS experiments at slightly different pressures and decompressing a crystallizing magma body to varying degrees had minimal effects on compositional evolution and phases crystallized.

Except for amphibole, the modeled crystallization temperatures, and abundances of minerals in these MELTS experiments are consistent with temperature estimates from the mineral thermobarometers (Fig. 13). Plagioclase starts to crystallize at 1060 °C, within error of the ~1050 °C highest temperatures estimated by the plagioclase + liquid thermometer of Putirka (2008) for PU-04-05 D. Ilmenite is the last phase to crystallize in very low abundances at 820 °C, consistent with the ~810 °C lowest estimates from the Fe—Ti oxide thermometer of Ghiorso and Evans (2008). Amphiboles contain many cations relative to other minerals, including an OH group, thus inferring temperatures and pressures from this mineral is challenging (e.g., Shane and Smith, 2013; Bechon et al.,

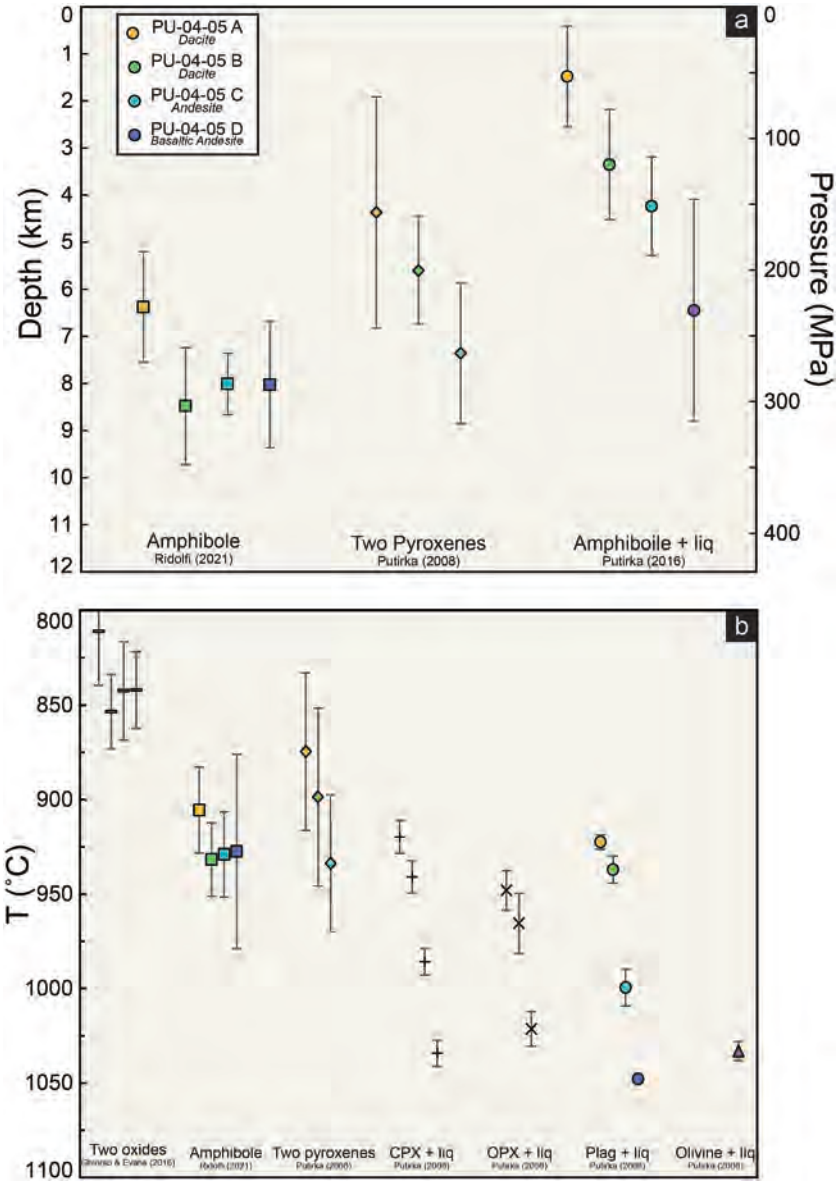

Fig. 11. Average pressure (A) and temperature (B) estimates from thermobarometry of mineral compositions. Vertical bars show internal ±1σ uncertainty for each thermometer or barometer. The average compositions of the phases used to estimate temperature or pressure are based on measurements in the Supplementary Materials Tables S3–S8. A total of 279 amphibole, 254 plagioclase, 65 clinopyroxene, 43 orthopyroxene, 54 olivine, 44 ilmenite-titanomagnetite pairs, and 176 glass measurements were used as described in section 4.3 of the text. The two pyroxene temperatures were calculated by pairing each clinopyroxene with each orthopyroxene that satsify equilibrium K_d constraints for each of the three Tephra samples using the algorith of Wieser et al. (2022).

2022). This holds for using amphibole compositions in barometers and thermometers of Ridolfi (2021) and Putirka (2008), as well as numerical MELTS models of hydrous systems (Ghiorso and Sack, 1995; Gualda et al., 2012). Thus, it is perhaps not surprising that our MELTS models crystallize amphibole at temperatures ~150 °C lower than estimates using Ridolfi (2021). Importantly, the average SiO_2/MgO ratios of orthopyroxene and clinopyroxene predicted in the MELTS simulation starting with 4 wt% H_2O are 1.8 and 2.9, respectively, whereas the amphibole averages 2.2. Thus, the crystallization of either two pyroxenes or amphibole will similarly impact the SiO_2/MgO ratio of evolving melts (e.g. Andersen et al., 2017). Although the prediction of pyroxene rather than amphibole crystallization may induce some model misfit, with caution we suggest that the agreement between the MELTS modeling (Fig. 13) and amphibole barometry (Fig. 11) indicates that the MELTS simulation yields useful first-order constraints on the storage and crystallization of the Paso Puyehue magma.

In summary, we find the whole-rock and glass compositions comprising the Paso Puyehue Tephra (Fig. 7), in parallel with the ubiquitous normal zoning of plagioclase (Fig. 10) and Rayleigh fractional crystallization models (Fig. 8) to be consistent with an origin of dacitic magma and rhyolite melts via extensive crystallization of water-rich basaltic andesite parent magma at pressures of 3 to 2.5 kbar, corresponding to 8 to 6.5 km depth. The MELTS models of magma reservoir evolution are by and large consistent with the temperature, pressure, water content, and oxidation state estimates that derive from the measured mineral compositions. On the other hand, evidence for the mixing of basaltic andesitic and dacitic magma is limited and may reflect hybridization across the interface between deeply stored basaltic andesite and overlying dacitic magma during destabilization, ascent, and eruption of the compositionally zoned magma body.

5.2. *Evolution of the Paso Puyehue magma reservoir*

We propose the following model (Fig. 14) for the generation of the

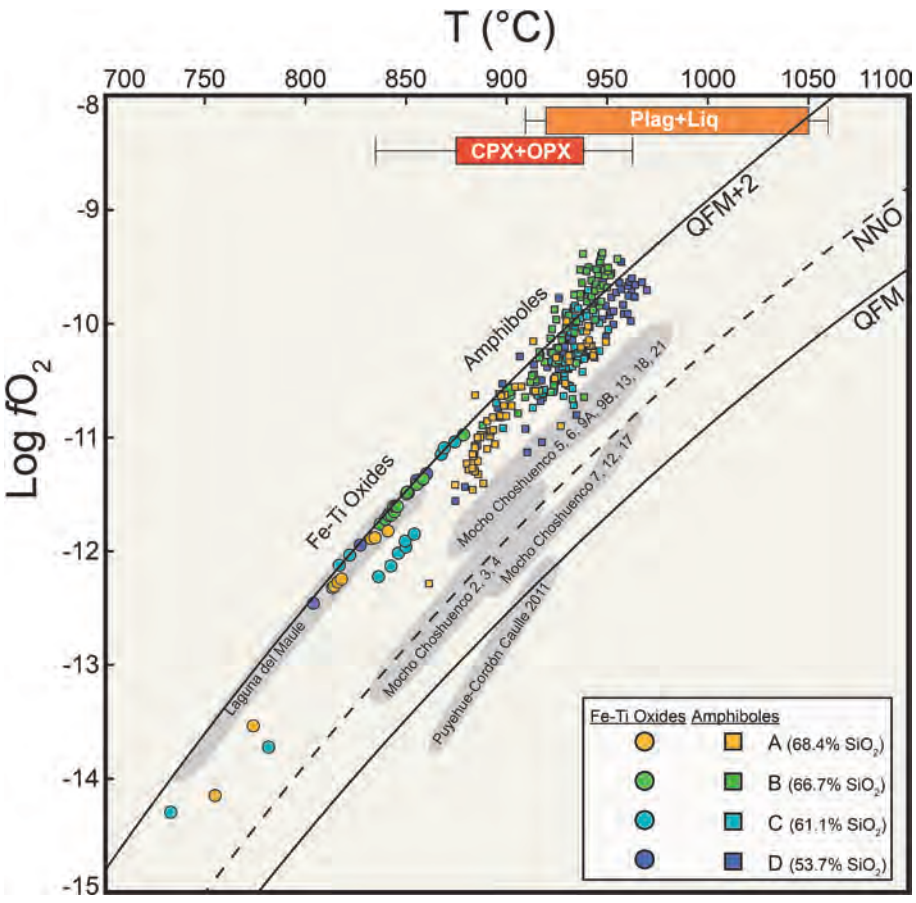

Fig. 12. Temperature and fO_2 estimates from magnetite-ilmenite pairs (colored circles) (Ghiorso and Evans, 2008). Colored squares are estimates from amphiboles, (Ridolfi, 2021). Estimated temperatures from plagioclase-liquid and two pyroxene thermometry (Putirka, 2008) are shown at top. The gray fields are for other SVZ rhyolitic eruptions including at Launa del Maule (Andersen et al., 2017). Post last glacial maximum fields for Mocho Choshuenco Tephra data are from Rawson et al. (2015). Using the Rawson et al. (2015) nomenclature: MC4 = Neltume rhyolite, MC5 = Pirehueico, MC9 = Huilo, MC18 = Hua-Hum, and MC21 = Pilmaiquén. The 2011 Cordón-Caulle rhyolite Tephra data are from Castro et al. (2013).

Table 2
Results of Ilmenite-titanomagnetite thermometry, amphibole barometry, and plagioclase hygrometry from the Paso Puyehue Tephra samples in Figs. 3D and 4. Calculated uncertainties are ±1σ of the estimate.

Sample	wt% SiO_2	T (°C)[1]	±	P (MPa)[2]	±	H_2O_{melt} (wt%)[3]	±	fO_2[1]	±
PU-04-05 A	68.5	811.0	28.6	236.1	43.5	3.76	0.1	−12.5	0.8
PU-04-05 B	66.7	853.4	19.6	314.1	45.9	3.64	0.1	−11.5	0.4
PU-04-05C	61.1	842.4	26.0	296.7	24.2	3.29	0.2	−11.9	0.7
PU-04-05 D	53.7	842.0	20.3	297.2	49.5	3.74	0.2	−11.7	0.4

[1] Two-oxides, Ghiorso and Evans (2008).
[2] Amphibole only, Ridolfi (2021).
[3] Plagioclase-liquid, Waters and Lange (2015).

zoned Paso Puyehue magma: (1) Basaltic magma generated in a deep crustal MASH zone (Hildreth and Moorbath, 1988) rose through the transcrustal plumbing system and crystallized to generate hornblende-bearing basaltic andesite at 8 km depth and 1050 °C, (2) protracted storage with coeval extraction of rhyolitic melt produced a lens of crystal-poor dacitic magma extending to 6.5 km depth at temperatures down to 850–810 °C atop an ever more crystal-rich basaltic andesitic mush, and (3) destabilization of the compositionally zoned magma reservoir, perhaps due to exsolution of H_2O and pressurization with limited *syn*-eruptive mixing between basaltic andesite and dacite during ascent within the conduit. Experiments of Rutherford and Hill (1993) on Mt. St. Helens dacite suggest that the thickness of reaction rims on amphibole, similar to those on crystals in the basaltic andesite scoria (Fig. 6H), are a function of magma ascent rate and loss of H_2O dissolved in the melt upon eruption. We suggest that the Paso Puyehue basaltic andesite ascended, decompressed and exolved H_2O more slowly and to a greater extent than did the the overlying dacite leading to the widespread occurrence of reaction rims on amphibole in this portion of the deposit (Fig. 6a).

Mixing of basaltic or basaltic andesitic magma into silicic magma is commonly cited as a mechanism for triggering explosive silicic eruptions (e.g., Sparks et al., 1977; Singer et al., 2016). The absence of evidence favoring magma mixing leads us to suggest that instead the highly explosive nature of the Paso Puyehue eruption reflects overpressurization due to the exsolution of H_2O from dacitic to rhyolitic melt. The exsolution of H_2O could have been propelled by either crystallization of the magma that drove up the concentration of volatiles in the melt phase (e.g., Arzilli et al., 2019), or slow decompression

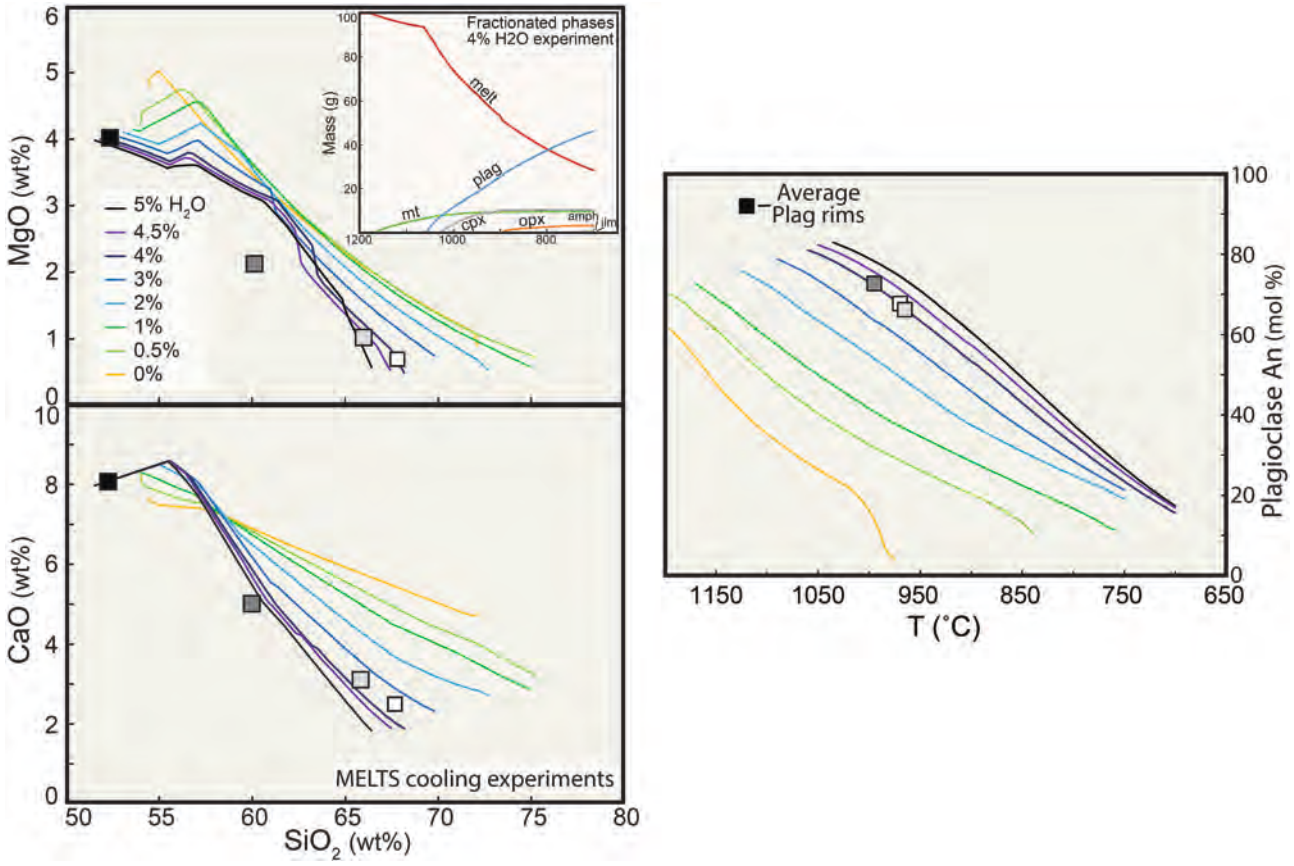

Fig. 13. MELTS isobaric fractional crystallization experiment results. Variation diagrams and plotted liquid lines of descent of different MELTS experiments for (A) Mg vs. SiO_2 and (B) Ca vs SiO_2. Each line is a numerical experiment at a different weight % H_2O, starting at the bulk composition of PU-04-05 D normalized for the H_2O of each experiment (this accounts for the offsets of the starting points of the numerical models from the black square). (C) The same fractional crystallization MELTS experiments, plotting crystallized feldspar content vs. temperature. The observed feldspar rim compositions plot along the liquid line of descent that assumes 4 wt% H_2O dissolved into the parent magma.

associated with magma ascent (Shea et al., 2009). The absence of reaction rims on euhedral amphibole crystals in the Paso Puyehue dacite (Fig. 6) argues against protracted decompression (Rutherford and Hill, 1993) and leads us to favor a model of crystallization-driven overpressurization.

Multiple lines of evidence support the extraction of rhyolitic melt from an underlying basaltic andesitic parent magma to generate the strong compositional zonation of the Paso Puyehue Tephra. The Paso Puyehue Tephra contains gabbroic glomerocrysts (Fig. 6C) in the andesitic and basaltic andesitic portions of the deposit, which we interpret as tiny fragments of the underlying, and largely unerupted, crystal mush (e.g., Winslow et al., 2022). Minerals, particularly plagioclase, are pervasively normally zoned (Fig. 9), suggesting a thermally buffered or cooling system that was not disturbed by the recharge of hot basaltic magma. Relatively large crystal sizes (up to 3 mm), euhedral faces, and intergrown crystals of pyroxene, plagioclase, and olivine in glomerocrysts suggest prolonged cooling and crystal growth reflective of crystal mush formation (e.g., Hammer, 2008; Holness et al., 2019).

Fractionation of a basaltic or basaltic andesitic magma to produce a silicic melt and leave behind a gabbroic crystal mush is important in generating chemical and thermal stratification, as documented here and at Puyehue-Cordón Caulle (Jay et al., 2014; Winslow et al., 2022). The Paso Puyehue Tephra deposit presents many similarities in origin to the historical rhyolite eruptions from Puyehue-Cordón Caulle, however, important differences in eruptive products and storage conditions between the two are discussed below.

5.3. Comparisons to other strongly compositionally zoned eruptions

Compositionally bimodal eruptive products within the SVZ have been explored at Volcán Melimoyu in the La Junta Tephra (Geoffroy et al., 2018), the Lepué Tephra, sourced from Volcán Michimahuida (Alloway et al., 2017), a zoned Holocene lava flow at Volcán San Pedro (Costa and Singer, 2002), the 1991 Volcán Hudson eruption (Kratzmann et al., 2009; Weller et al., 2014), the 1932 lava and Tephra emitted from Volcán Quizapu (Ruprecht et al., 2012) and mafic enclaves in 2011 rhyolite lava flows from Puyehue-Cordón Caulle (Winslow et al., 2022). A compositionally bimodal Holocene Tephra has also been recognized on Osorno volcano (Geoffroy et al., 2018; Fig. 1). Each of these eruptions brought to the surface both basaltic to basaltic andesitic and dacitic to rhyolitic magmas with compositional gaps separating endmembers. Some of these examples are shown to originate dominantly by recharge injection of basalt into silicic magma and subsequent mixing (Costa and Singer, 2002; Kratzmann et al., 2009; Weller et al., 2014; Geoffroy et al., 2018), whereas others are interpreted as the products of fractional crystallization with a minimal role for magma recharge and mixing (Alloway et al., 2017; Ruprecht et al., 2012; Winslow et al., 2022).

The 2011 rhyolite eruption from Puyehue-Cordón Caulle (Castro et al., 2013; Jay et al., 2014; Winslow et al., 2022) invites further comparison with the Paso Puyehue Tephra. Both systems can be explained by the extraction of rhyolitic melt from an underlying crystal-rich mush of basaltic andesitic composition. This mechanism produces an overlying layer of crystal-poor silicic melt via protracted cooling and fractional crystallization of underlying magma (Winslow et al., 2022). However, there are significant differences between

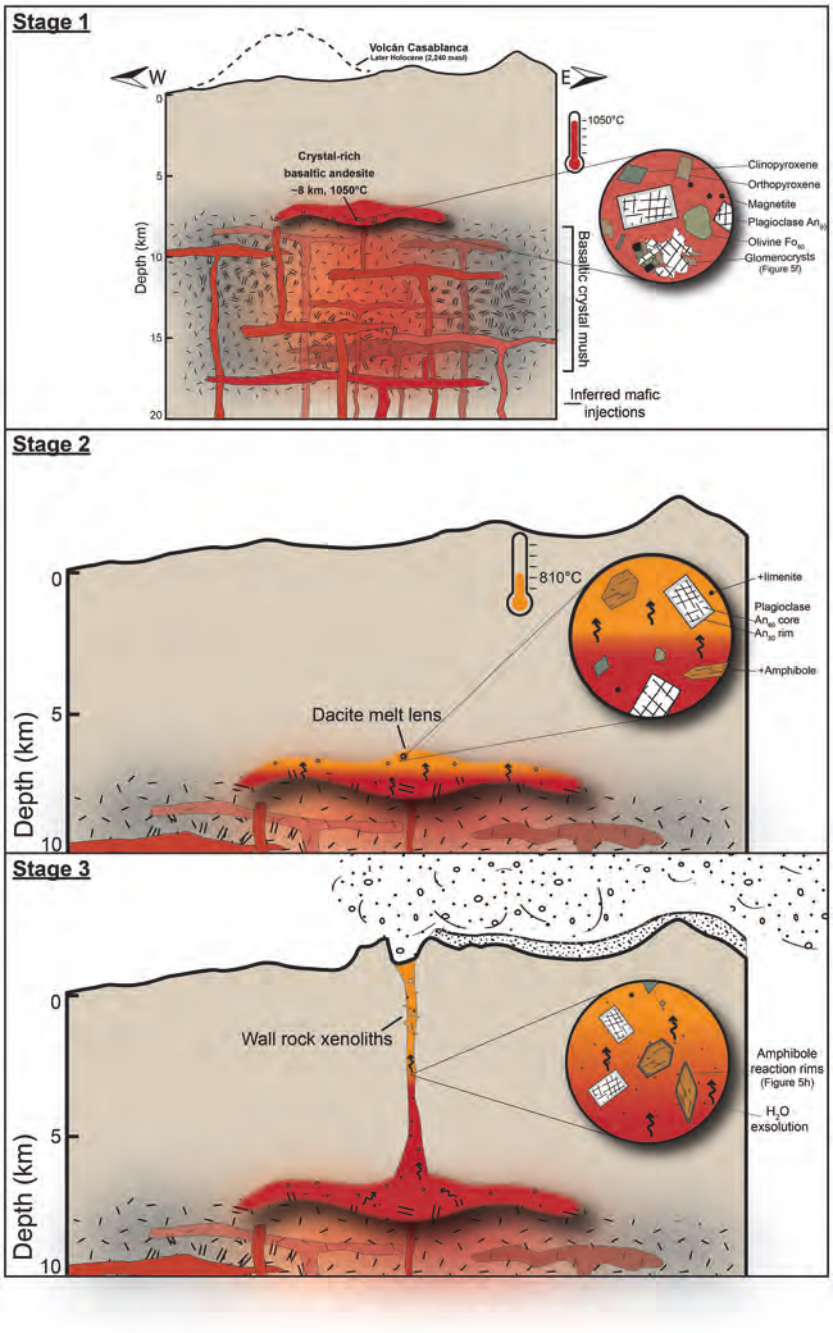

Fig. 14. Model of the evolution of the Paso Puyehue magma reservoir beneath the Antillanca Volcanic Complex, (1) during the formation of a basaltic andesite crystal mush at 8 km depth with temperatures as high as 1050 °C, (2) protracted cooling and extraction of an overlying, cooler dacitic melt lens from the basaltic andesitic crystal mush at temperatures as low as 810 °C and 6.5 km depth, and (3) saturation and exsolution of H_2O, with limited mixing between the basaltic andesite and dacite upon eruption.

eruptive products and magma storage conditions. The Paso Puyehue Tephra contains amphibole, whereas no lava or tephra from Puyehue-Cordón Caulle does (Singer et al., 2008). Experiments on the 2011 rhyolite erupted from Cordón Caulle, as well as plagioclase-hosted melt inclusion H_2O contents of 0.74 to 2.4 wt% H_2O, indicates that it was stored between about 5.0 and 2.5 km (Castro et al., 2013; Seropian et al., 2021), which is 2–3 km less than the 8.0–6.5 km depths we have inferred for the Paso Puyehue magma body. Moreover, the Paso Puyehue magma is highly oxidized along the QFM + 2 buffer, compared to the 2011 Cordón Caulle rhyolite, below the QFM buffer (Fig. 12; Castro et al., 2013). The contrast in storage depths of the relatively dry 2011 Cordón Caulle rhyolite and the wetter Paso Puyehue dacite are consistent with deeper ponding, crystallization, and viscosity increases within H_2O-saturated magmas proposed by Rasmussen et al. (2022).

The likely cause of highly oxidized magma to produce the Paso Puyehue Tephra is enhanced H_2O in melts within the sub-AVC magma plumbing system. We estimate the dissolved H_2O concentration within the basaltic andesite portion of the Paso Puyehue reservoir at about 4 wt %, resulting in the stabilization of amphibole. Extensive crystal fractionation of this parent magma would push melt H_2O concentrations in Paso Puyehue dacite even higher as our melts models suggest. In subduction zones, Kelley and Cottrell (2009) infer a direct link between H_2O mass transfer from the subducted plate and oxidation of the mantle wedge, thus, we suggest the oxidized magma plumbing system beneath

the AVC reflects water concentrations in melts that are greater than those within the Puyehue-Cordón Caulle plumbing system. Higher melt H_2O concentrations can decrease magma viscosity by orders of magnitude but also lead to volatile exsolution that can, in turn, increase magma viscosity. Despite increasing magma viscosity, the exsolution of volatiles can make extraction of rhyolitic melt from crystal-rich mush highly efficient (Parmigiani et al., 2016; Hartung et al., 2019). A higher H_2O content and exsolution of copious H_2O may explain why the Paso Puyehue reservoir contained co-eruptive quantities of both the basaltic andesitic and dacitic magma that produced a strongly zoned tephra deposit. In contrast, the dryer more viscous magma reservoir beneath Cordón Caulle resulted in an eruption of rhyolite, with minuscule amounts of the underlying basaltic andesite entrained in effusively erupted lava as rare gabbroic enclaves (Winslow et al., 2022).

6. Conclusions

The eruption of compositionally bimodal magma during the Holocene is more common at many volcanic centers along the SVZ than previously thought. Examples of basaltic recharge and mixing into rhyolitic reservoirs are many. In contrast, our results show the growth of a zoned Paso Puyehue magma body occurred mainly by fractional crystallization and extraction of silicic melt from underlying basaltic andesite magma. Pervasive normal zoning at the rims of plagioclase crystals and trace element compositions are consistent with simple Rayleigh fractional crystallization models. MELTS numerical models show that fractional crystallization of a basaltic andesite parent with 4 wt% H_2O generates the observed dacite magma composition and mineralogy via 40–60% crystallization. We suggest that volatile saturation at shallow depth due to crystallization, not destabilization by injection of a recharge magma, triggered the upward mobilization and explosive eruption to generate the Paso Puyehue Tephra. The Paso Puyehue magma body was highly oxidized compared to eruptions from other SVZ volcanoes, likely due to the enhanced delivery of dissolved H_2O into the mantle wedge from the subducting slab. A relatively hydrous mantle wedge and magma plumbing system may explain why the Paso Puyehue Tephra co-erupted both rhyolite and underlying basaltic andesitic magma, whereas the dryer, less oxidized 2011 Cordón Caulle eruption only contained trace amounts of entrained gabbroic enclaves erupted within the effusive rhyolite lava. These differences likely reflect contrasts in the dynamics of how viscosity and density evolve within crystal mushes and their interstitial melts in wetter vs. dryer systems.

Author statement

Cam DeSilva, Brad Singer, Brent V. Alloway, and Pablo Moreno-Yaeger are authors of this manuscript.

Declaration of Competing Interest

The authors declare the following financial interests/personal relationships which may be considered as potential competing interests:

Brad Singer reports financial support was provided by US NSF.

Data availability

All data is in the Supplementary Files

Acknowledgments

This work comprises the MSc thesis of DeSilva. Supported in part by U.S. NSF grant EAR-2121570 plus a Vilas Professorship (Singer) and the Geoscience Department at the University of Wisconsin-Madison. The Antillanca Ski Center provided lodging and logistical support. We thank Gustavo Villarosa (CONICET-Universidad Nacional del Comahue, Argentina) for his generous assistance in deciding a new and appropriate geographical name for the regionally distinct Paso Puyehue Tephra. We are grateful for the assistance of Bryan Wathen and Drae Rogers in sample preparation as well as Will Nachlas and Bil Schneider for their assistance in acquiring mineral and glass compositions. Two anonymous reviews helped us to improve the clarity of this paper. We thank the Reserva Nacional Puyehue of Corporacion Nacional Forestal (CONAF) for permission to work in protected areas.

Appendix A. Supplementary data

Supplementary data to this article can be found online at https://doi.org/10.1016/j.jvolgeores.2023.107943.

References

Alloway, B.V., Moreno, P.I., Pearce, N.J., De Pol-Holz, R., Henríquez, W.I., Pesce, O.H., Sagredo, E., Villarosa, G., Outes, V., 2017. Stratigraphy, age and correlation of Lepué tephra: a widespread c. 11 000 cal a BP marker horizon sourced from the Chaitén Sector of southern Chile. J. Quat. Sci. 32 (6), 795–829. https://doi.org/10.1002/jqs.2976.

Alloway, B.V., Pearce, N.J., Moreno, P.I., Villarosa, G., Jara, I.A., Henríquez, C.A., Outes, V., 2022. Refinement of the tephrostratigraphy straddling the northern Patagonian Andes (40–41° S): new tephra markers, reconciling different archives and ascertaining the timing of piedmont deglaciation. J. Quat. Sci. 37 (3), 441–477. https://doi.org/10.1016/j.quascirev.2017.05.011.

Andersen, N.L., Jicha, B.R., Singer, B.S., Hildreth, W., 2017. Incremental heating of Bishop Tuff sanidine reveals preeruptive radiogenic Ar and rapid remobilization from cold storage. Proc. Natl. Acad. Sci. 114 (47), 12407–12412.

Arzilli, F., Morgavi, D., Petrelli, M., Polacci, M., Burton, M., Di Genova, D., Spina, L., La Spina, G., Hartley, M.E., Romero, J.E., Fellowes, J., 2019. The unexpected explosive sub-Plinian eruption of Calbuco volcano (22–23 April 2015; southern Chile): triggering mechanism implications. J. Volcanol. Geotherm. Res. 378, 35–50.

Asimow, P.D., Ghiorso, M.S., 1998. Algorithmic modifications extending MELTS to calculate subsolidus phase relations. Am. Mineral. 83 (9–10), 1127–1132. https://doi.org/10.2138/am-1998-9-1022.

Bacon, C.R., Druitt, T.H., 1988. Compositional evolution of the zoned calc-alkaline magma chamber of Mount Mazama, Crater Lake, Oregon. Contrib. Mineral. Petrol. 98, 224–256. https://doi.org/10.1007/BF00402114.

Bacon, C.R., Hirschmann, M.M., 1988. Mg/Mn partitioning as a test for equilibrium between coexisting Fe-Ti oxides. Am. Mineral. 73 (1–2), 57–61.

Bacon, C.R., Metz, J., 1984. Magmatic inclusions in rhyolites, contaminated basalts, and compositional zonation beneath the Coso volcanic field, California. Contrib. Mineral. Petrol. 85, 346–365. https://doi.org/10.1007/BF01150292.

Bechon, T., Billon, M., Namur, O., Bolle, O., Fugmann, P., Foucart, H., Vander Auwera, J., 2022. Petrology of the magmatic system beneath Osorno volcano (Central Southern Volcanic Zone, Chile). Lithos 426, 106777. https://doi.org/10.1016/j.lithos.2022.106777.

Brophy, J.G., 1991. Composition gaps, critical crystallinity, and fractional crystallization in orogenic (calc-alkaline) magmatic systems. Contrib. Mineral. Petrol. 109 (2), 173–182. https://doi.org/10.1007/BF00306477/METRICS.

Carrasco Lira, C.A., 2016. Petrología y geoquímica del volcán Casablanca y centros eruptivos cercanos, Complejo volcánico Antillanca, Región de Los Lagos, Chile. Memoria thesis,. Universidad de Chile, Santiago, 109 pp.

Cashman, K.V., Sparks, R.S.J., Blundy, J.D., 2017. Vertically extensive and unstable magmatic systems: a unified view of igneous processes. Science 355 (6331), eaag3055. https://doi.org/10.1126/science.aag3055.

Castro, J.M., Schipper, C.I., Mueller, S.P., Militzer, A.S., Amigo, A., Parejas, C.S., Jacob, D., 2013. Storage and eruption of near-liquidus rhyolite magma at Cordón Caulle, Chile. Bull. Volcanol. 75, 1–17.

Cembrano, J., Lara, L., 2009. The link between volcanism and tectonics in the southern volcanic zone of the Chilean Andes: a review. Tectonophysics 471 (1–2), 96–113. https://doi.org/10.1016/j.tecto.2009.02.038.

Conrey, R.M., Bailey, D.G., Singer, J.W., Wagoner, L.J., Parfitt, B., Hay, J., Keh, O., Chang, Z., Huang, S., 2023. *Combined use of multiple external and internal standards in LA-ICP-MS analysis of bulk geological samples using lithium borate fused glass*. Geochem.: Explor. Environ. Anal. 23 (2) https://doi.org/10.1144/geochem2023-001 geochem2023-001.

Cooper, K.M., Kent, A.J., 2014. Rapid remobilization of magmatic crystals kept in cold storage. Nature 506 (7489), 480–483. https://doi.org/10.1038/nature12991.

Costa, F., Singer, B., 2002. Evolution of Holocene dacite and compositionally zoned magma, Volcán San Pedro, southern volcanic zone, Chile. J. Petrol. 43 (8), 1571–1593. https://doi.org/10.1093/petrology/43.8.1571.

Daly, R.A., 1925. The geology of Ascension Island. In: Proceedings of the American Academy of Arts and Sciences, 60, pp. 3–80. https://doi.org/10.2307/25130043.

Davidson, J., Turner, S., Handley, H., Macpherson, C., Dosseto, A., 2007. Amphibole "sponge" in arc crust? Geology 35 (9), 787–790. https://doi.org/10.1130/G23637A.1.

Droop, G.T.R., 1987. A general equation for estimating Fe3+ concentrations in ferromagnesian silicates and oxides from microprobe analyses, using stoichiometric criteria. Mineral. Mag. 51 (361), 431–435. https://doi.org/10.1180/minmag.1987.051.361.10.

Dufek, J., Bachmann, O., 2010. Quantum magmatism: Magmatic compositional gaps generated by melt-crystal dynamics. Geology 38 (8), 687–690. https://doi.org/10.1130/G30831.1.

Eichelberger, J.C., Chertkoff, D.G., Dreher, S.T., Nye, C.J., 2000. Magmas in collision: rethinking chemical zonation in silicic magmas. Geology 28 (7), 603–606. https://doi.org/10.1130/0091-7613(2000)028<0603:MICRCZ>2.3.CO;2.

Ganne, J., Bachmann, O., Feng, X., 2018. Deep into magma plumbing systems: Interrogating the crystal cargo of volcanic deposits. Geology 46 (5), 415–418. https://doi.org/10.1130/G39857.1.

Geoffroy, C.A., Alloway, B.V., Amigo, À., Parada, M.A., Gutierrez, F., Castruccio, A., Moreno, P.I., 2018. A widespread compositionally bimodal tephra sourced from Volcán Melimoyu (44° S, Northern Patagonian Andes): Insights into magmatic reservoir processes and opportunities for regional correlation. Quat. Sci. Rev. 200, 141–159. https://doi.org/10.1016/j.quascirev.2018.09.034.

Ghiorso, M.S., Evans, B.W., 2008. Thermodynamics of rhombohedral oxide solid solutions and a revision of the Fe-Ti two-oxide geothermometer and oxygen-barometer. Am. J. Sci. 308 (9), 957–1039. https://doi.org/10.2475/09.2008.01.

Ghiorso, M.S., Sack, R.O., 1995. Chemical mass transfer in magmatic processes IV. A revised and internally consistent thermodynamic model for the interpolation and extrapolation of liquid-solid equilibria in magmatic systems at elevated temperatures and pressures. Contrib. Mineral. Petrol. 119, 197–212. https://doi.org/10.1007/BF00307281.

Grove, T.L., Baker, M.B., 1984. Phase equilibrium controls on the tholeiitic versus calc-alkaline differentiation trends. J. Geophys. Res. Solid Earth 89 (B5), 3253–3274. https://doi.org/10.1029/JB089iB05p03253.

Gualda, G.A., Ghiorso, M.S., Lemons, R.V., Carley, T.L., 2012. Rhyolite-MELTS: a modified calibration of MELTS optimized for silica-rich, fluid-bearing magmatic systems. J. Petrol. 53 (5), 875–890. https://doi.org/10.1093/petrology/egr080.

Hammer, J.E., 2008. Experimental studies of the kinetics and energetics of magma crystallization. Rev. Mineral. Geochem. 69 (1), 9–59. https://doi.org/10.2138/rmg.2008.69.2.

Hartung, E., Weber, G., Caricchi, L., 2019. The role of H_2O on the extraction of melt from crystallising magmas. Earth Planet. Sci. Lett. 508, 85–96. https://doi.org/10.1016/j.epsl.2018.12.010.

Hickey-Vargas, R., Holbik, S., Tormey, D., Frey, F.A., Roa, H.M., 2016. Basaltic rocks from the Andean Southern Volcanic Zone: Insights from the comparison of along-strike and small-scale geochemical variations and their sources. Lithos 258, 115–132. https://doi.org/10.1016/J.LITHOS.2016.04.014.

Hildreth, W., 1981. Gradients in silicic magma chambers: implications for lithospheric magmatism. J. Geophys. Res. Solid Earth 86 (B11), 10153–10192. https://doi.org/10.1029/JB086iB11p10153.

Hildreth, W., 1983. The compositionally zoned eruption of 1912 in the valley of ten thousand smokes, Katmai National Park, Alaska. J. Volcanol. Geotherm. Res. 18 (1–4), 1–56. https://doi.org/10.1016/0377-0273(83)90003-3.

Hildreth, W., Drake, R.E., 1992. Volcán Quizapu, Chilean Andes. Bull. Volcanol. 54, 93–125. https://doi.org/10.1007/BF00278002.

Hildreth, W., Fierstein, J., 2012. The Novarupta-Katmai eruption of 1912: largest eruption of the twentieth century: centennial perspectives. In: USGS Professional Paper 1791, 259 pp Available at. https://pubs.usgs.gov/pp/1791/.

Hildreth, W., Moorbath, S., 1988. Crustal contributions to arc magmatism in the Andes of Central Chile. Contrib. Mineral. Petrol. 98, 455–489. https://doi.org/10.1007/BF00372365.

Holness, M.B., Stock, M.J., Geist, D., 2019. Magma chambers versus mush zones: constraining the architecture of sub-volcanic plumbing systems from microstructural analysis of crystalline enclaves. Phil. Trans. R. Soc. A 377 (2139), 20180006. https://doi.org/10.1098/rsta.2018.0006.

Humphreys, M.C., Blundy, J.D., Sparks, R.S.J., 2006. Magma evolution and open-system processes at Shiveluch Volcano: insights from phenocryst zoning. J. Petrol. 47 (12), 2303–2334. https://doi.org/10.1093/petrology/egl045.

Jackson, M.D., Blundy, J., Sparks, R.S.J., 2018. Chemical differentiation, cold storage and remobilization of magma in the Earth's crust. Nature 564 (7736), 405–409. https://doi.org/10.1038/s41586-018-0746-2.

Jay, J., Costa, F., Pritchard, M., Lara, L., Singer, B., Herrin, J., 2014. Locating magma reservoirs using InSAR and petrology before and during the 2011–2012 Cordón Caulle silicic eruption. Earth Planet. Sci. Lett. 395, 254–266. https://doi.org/10.1016/j.epsl.2014.03.046.

Kelley, K.A., Cottrell, E., 2009. Water and the oxidation state of subduction zone magmas. Science 325 (5940), 605–607. https://doi.org/10.1126/science.1174156.

Kratzmann, D.J., Carey, S., Scasso, R., Naranjo, J.A., 2009. Compositional variations and magma mixing in the 1991 eruptions of Hudson volcano, Chile. Bull. Volcanol. 71, 419–439. https://doi.org/10.1007/s00445-008-0234-x.

Mixon, E.E., Singer, B.S., Jicha, B.R., Ramirez, A., 2021. Calbuco, a monotonous andesitic high-flux volcano in the Southern Andes, Chile. J. Volcanol. Geotherm. Res. 416, 107279 https://doi.org/10.1016/j.jvolgeores.2021.107279.

Moore, H.C., Carey, R.J., Houghton, B.F., Jutzeler, M., White, J.D., 2022. High-temperature oxidation of proximal basaltic pyroclasts, 1886 Tarawera, New Zealand. Bull. Volcanol. 84, 46.

Murphy, M.A., Salvador, A., 1999. International stratigraphic guide—an abridged version. Episodes J. Int. Geosci. 22, 255–271. https://doi.org/10.18814/epiiugs/1999/v22i4/002.

Naranjo, J.A., Singer, B.S., Jicha, B.R., Moreno, H., Lara, L.E., 2017. Holocene tephra succession of Puyehue-Cordón Caulle and Antillanca/Casablanca volcanic complexes, southern Andes (40–41 S). J. Volcanol. Geotherm. Res. 332, 109–128. https://doi.org/10.1016/j.jvolgeores.2016.11.017.

Parmigiani, A., Faroughi, S., Huber, C., Bachmann, O., Su, Y., 2016. Bubble accumulation and its role in the evolution of magma reservoirs in the upper crust. Nature 532 (7600), 492–495. https://doi.org/10.1038/nature17401.

Putirka, K.D., 2008. Thermometers and barometers for volcanic systems. Rev. Mineral. Geochem. 69 (1), 61–120. https://doi.org/10.2138/RMG.2008.69.3.

Putirka, K., 2016. Amphibole thermometers and barometers for igneous systems and some implications for eruption mechanisms of felsic magmas at arc volcanoes. Am. Mineral. 101 (4), 841–858. https://doi.org/10.2138/am-2016-5506.

Rasmussen, D.J., Plank, T.A., Roman, D.C., Zimmer, M.M., 2022. Magmatic water content controls the pre-eruptive depth of arc magmas. Science 375 (6585), 1169–1172. https://doi.org/10.1126/science.abm5174.

Rawson, H., Naranjo, J.A., Smith, V.C., Fontijn, K., Pyle, D.M., Mather, T.A., Moreno, H., 2015. The frequency and magnitude of post-glacial explosive eruptions at Volcán Mocho-Choshuenco, southern Chile. J. Volcanol. Geotherm. Res. 299, 103–129.

Ridolfi, F., 2021. Amp-TB2: an updated model for calcic amphibole thermobarometry. Minerals 11 (3), 324. https://doi.org/10.3390/min11030324.

Ruprecht, P., Bergantz, G.W., Cooper, K.M., Hildreth, W., 2012. The crustal magma storage system of Volcán Quizapu, Chile, and the effects of magma mixing on magma diversity. J. Petrol. 53, 801–840. https://doi.org/10.1093/petrology/egs002.

Rutherford, M.J., Hill, P.M., 1993. Magma Ascent rates from amphibole breakdown: an experimental study applied to the 1980-1986 Mount St. Helens Eruptions (Paper 93JB01613). J. Geophys. Res. 98, 19–667. https://doi.org/10.1029/93JB01613.

Seropian, G., Schipper, C.I., Harmon, L.J., Smithies, S.L., Kennedy, B.M., Castro, J.M., Forte, P., 2021. A century of ongoing silicic volcanism at Cordón Caulle, Chile: new constraints on the magmatic system involved in the 1921–1922, 1960 and 2011–2012 eruptions. J. Volcanol. Geotherm. Res. 420, 107406 https://doi.org/10.1016/j.jvolgeores.2021.107406.

Shane, P., Smith, V.C., 2013. Using amphibole crystals to reconstruct magma storage temperatures and pressures for the post-caldera collapse volcanism at Okataina volcano. Lithos 156, 159–170.

Shea, T., Larsen, J.F., Gurioli, L., Hammer, J.E., Houghton, B.F., Cioni, R., 2009. Leucite crystals: surviving witnesses of magmatic processes preceding the 79AD eruption at Vesuvius, Italy. Earth Planet. Sci. Lett. 281, 88–98.

Singer, B.S., Jicha, B.R., Harper, M.A., Naranjo, J.A., Lara, L.E., Moreno-Roa, H., 2008. Eruptive history, geochronology, and magmatic evolution of the Puyehue-Cordón Caulle volcanic complex, Chile. Geol. Soc. Am. Bull. 120, 599–618. https://doi.org/10.1130/B26276.1.

Singer, B.S., Costa, F., Herrin, J.S., Hildreth, W., Fierstein, J., 2016. The timing of compositionally zoned magma reservoirs and mafic 'priming' weeks before the 1912 Novarupta-Katmai rhyolite eruption. Earth Planet. Sci. Lett. 451, 125–137. https://doi.org/10.1016/j.epsl.2016.07.015.

Sparks, S.R., Sigurdsson, H., Wilson, L., 1977. Magma mixing: a mechanism for triggering acid explosive eruptions. Nature 267, 315–318.

Stern, C.R., 2004. Active Andean volcanism: its geologic and tectonic setting. Rev. Geol. Chile 31, 161–206. https://doi.org/10.4067/S0716-02082004000200001.

Villarosa, G., Outes, V., Hajduk, A., Montero, E.C., Sellés, D., Fernández, M., Crivelli, E., 2006. Explosive volcanism during the Holocene in the Upper Limay River Basin: the effects of ashfalls on human societies, Northern Patagonia, Argentina. Quat. Int. 158 (1), 44–57. https://doi.org/10.1016/j.quaint.2006.05.016.

Waters, L.E., Lange, R.A., 2015. An updated calibration of the plagioclase-liquid hygrometer-thermometer applicable to basalts through rhyolites. Am. Mineral. 100 (10), 2172–2184. https://doi.org/10.2138/am-2015-5232.

Weller, D., Miranda, C.G., Moreno, P.I., Villa-Martínez, R., Stern, C.R., 2014. The large late-glacial Ho eruption of the Hudson volcano, southern Chile. Bull. Volcanol. 76, 1–18. https://doi.org/10.1007/s00445-014-0831-9.

Wieser, P., Petrelli, M., Lubbers, J., Wieser, E., Ozaydin, S., Kent, A., Till, C., 2022. Thermobar: an open-source Python3 tool for thermobarometry and hygrometry. Volcanica 5 (2), 349–384. https://doi.org/10.30909/vol.05.02.349384.

Winslow, H., Ruprecht, P., Gonnermann, H.M., Phelps, P.R., Muñoz-Saez, C., Delgado, F., Pritchard, M., Amigo, A., 2022. Insights for crystal mush storage utilizing mafic enclaves from the 2011–12 Cordón Caulle eruption. Sci. Rep. 12 (1), 9734. https://doi.org/10.1038/s41598-022-13305-y.

Wolff, J.A., Ellis, B.S., Ramos, F.C., Starkel, W.A., Boroughs, S., Olin, P.H., Bachmann, O., 2015. Remelting of cumulates as a process for producing chemical zoning in silicic tuffs: a comparison of cool, wet and hot, dry rhyolitic magma systems. Lithos 236, 275–286. https://doi.org/10.1016/j.lithos.2015.09.002.